

The Effect of Zirconium Addition on the Mechanical Properties of High Temperature Titanium Alloy

M.Tech. Thesis

By

ROHIT R S



**DISCIPLINE OF METALLURGY ENGINEERING AND
MATERIALS SCIENCE**

**INDIAN INSTITUTE OF TECHNOLOGY
INDORE**

AUGUST, 2018

The Effect of Zirconium Addition on the Mechanical Properties of High Temperature Titanium Alloy

A THESIS

*Submitted in partial fulfilment of the requirements for the
award of the degree*

of
Master of Technology

by

ROHIT R S



**DISCIPLINE OF METALLURGY
ENGINEERING AND MATERIALS SCIENCE**

**INDIAN INSTITUTE OF
TECHNOLOGY INDORE**

AUGUST, 2018



INDIAN INSTITUTE OF TECHNOLOGY INDORE

CANDIDATE'S DECLARATION

I hereby certify that the work which is being presented in the thesis entitled **The Effect of Zirconium Addition on the Mechanical Properties of High Temperature Titanium Alloy** in the partial fulfilment of the requirements for the award of the degree of **MASTER OF TECHNOLOGY** and submitted in the **DISCIPLINE OF Metallurgy Engineering and Materials Science, Indian Institute of Technology Indore**, is an authentic record of my own work carried out during the time period from July 2016 to June 2018 under the supervision of Dr. Jayaprakash Murugesan, Assistant Professor, Discipline of Metallurgy Engineering and Materials Science.

The matter presented in this thesis has not been submitted by me for the award of any other degree of this or any other institute.

Signature of the student with date
ROHIT R S

This is to certify that the above statement made by the candidate is correct to the best of my knowledge.

Signature of the Supervisor
Date:
Dr. Jayaprakash Murugesan

ROHIT R S has successfully given his M.Tech Oral Examination held on

Signature of Supervisor of M.Tech thesis
Date:

Convener, DPGC
Date:

Signature of PSPC Member #1
Date:

Signature of PSPC Member #2
Date:

ACKNOWLEDGEMENTS

To complete this thesis, it required enormous effort and determination. However, successful result would not have been achieved if there was no help from very special people.

First of all, I would like to express my utmost gratitude to my supervisor, **Dr. Jayaprakash Murugesan**, who has consistently given me invaluable advice and knowledge. Working with him during the whole course of this thesis was an enjoyable and inspiring journey. I am indebted to him for the on-time completion of this thesis.

I take this opportunity to express my profound gratitude towards my PSPC members, **Dr. I A Palani** and **Dr. Mrigendra Dubey** for their guidance, support and cooperation. I am thankful to all the **faculty members** of the MEMS Discipline for their immense guidance and support.

I'm also thankful to the PhD students **Sangam Sangral, Mahesh Patel, Sheetal Dewangan, Priyanka Sahu and Aditya Litoria**, and my friends **Milind Kumar, Yeswanth Sai and Ankit Mishra**. Thank you guys for the useful discussion and friendship.

Finally, from the bottom of my heart I would like to express my deepest affection to my mother **Sarojini R** and my father **Dr. M S Rajan** for their endless encouragement and support.

ROHIT R S

.....*Dedicated to*

My

Parents

ABSTRACT

Titanium and its alloy have been widely used for aerospace application because of its high specific strength, good corrosion resistance, good fatigue, creep strength and etc. The development of high temperature titanium alloys have contributed significantly to the spectacular progress in thrust-to-weight ratio in aircraft gas turbines. Titanium alloys have comparatively low modulus, good fatigue strength, low density, high strength to weight ratio, formability, machinability, corrosion resistance, and biocompatibility. This thesis discusses an overview on the development of high-temperature titanium alloys for use in gas turbines.

Ti-Al-Zr-Sn-Mo-Si based near alpha titanium alloys are widely used in jet engine applications in the temperature range of 450°C – 600°C. To increase the operating temperature and to increase the high temperature strength of these alloys, numerous number of research works have been carried out. Alloying addition is one of the fundamental and effective methods to enhance the mechanical properties of titanium. Zirconium (Zr) is one of the effective solid solution strengtheners in titanium alloys. The effect of increase in zirconium content on high temperature strength of titanium alloys have not yet been extensively studied.

In the present study, the effect of increase in zirconium content has been studied on the properties of Ti-6Al-xZr-2Sn-0.5Mo-0.5Nb-0.3Si ($x = 2, 4, 6, 8$) based high temperature titanium alloy at room temperature and at 500 °C. The alloys were prepared in vacuum arc furnace under an argon atmosphere. The alloys were solution treated followed by ageing. The titanium alloys prepared were subjected to various characterization techniques like optical microscopy, tensile testing, hardness testing, wear and wear surface analysis, DSC and XRD. The microstructure revealed lamellae structures with the lath size decreasing with increasing Zr content. Tensile test was performed to find out the yield strength and UTS of each alloy, and their hardness were measured using

Rockwell hardness test. The rate of wear were analysed for each alloy, and the wear surfaces were examined using optical microscopy and roughness test. DSC analysis was used to check the transformation temperature of the alloys. XRD analysis was used to identify the phases formed in the alloys. The results showed that with an increase in zirconium content, the tensile strength at room temperature and at 500 °C, and hardness at room temperature increased significantly. The rate of wear was found to decrease with increase in Zr content in the alloys. The results obtained are discussed based on microstructure analysis using optical microscope. It is inferred that zirconium strengthens the Ti-6Al-xZr-2Sn-0.5Mo-0.5Nb-0.3Si at both room temperature and at high temperature (500 °C).

The results obtained from optical microscopy, tensile test, hardness test, wear and wear surface analyses, DSC and XRD would be helpful for the future development of new high temperature titanium alloys, which would be useful for reducing weight and better fuel consumption.

TABLE OF CONTENTS

LIST OF FIGURES	V
LIST OF TABLES	VII
NOMENCLATURE.....	IX
ACRONYMS	XI
Chapter 1 INTRODUCTION	1
1.1 Organization of the Thesis	3
Chapter 2 LITERATURE REVIEW	5
2.1 Introduction to Titanium	5
2.2 Alloying of Titanium.....	7
2.3 Classification of Titanium alloys	9
2.3.1 α alloys.....	11
2.3.2 $\alpha+\beta$ alloys	11
2.3.3 β alloys.....	15
2.4 Titanium in Aerospace	22
2.5 Titanium as Biomaterials	25
2.6 Review of Past Work.....	26
2.7 Identified Research Gap	27
2.8 Objectives of the Thesis	27
Chapter 3 EXPERIMENTAL TECHNIQUES	29
3.1 Alloy Development	29
3.2 Characterization	33
3.2.1 Microstructure Analysis	33
3.2.2 Tensile Test.....	36
3.2.3 Hardness Test	38
3.2.4 Wear Test.....	39
3.2.5 Roughness Test.....	42
3.2.6 Differential Scanning Calorimetry (DSC).....	44
3.2.7 X-Ray Diffraction (XRD).....	44

Chapter 4 RESULTS AND DISCUSSION	47
4.1 Optical Micrograph	47
4.2 Tensile Test	49
4.3 Hardness Test	54
4.4 Wear Analysis	55
4.5 Roughness Analysis	59
4.6 Differential Scanning Calorimetry (DSC).....	60
4.7 X-Ray Diffraction (XRD)	60
Chapter 5 CONCLUSION	63
5.1 Future Scope of this study.....	64
REFERENCES.....	65

LIST OF FIGURES

Figure 1.1: Research Methodology.....	3
Figure 2.1: Ti crystal structure (a) hcp (b) bcc	6
Figure 2.2: Schematic for solid solution strengthening with (a) small (b) large substitutional atoms; and (c) interstitial atoms	8
Figure 2.3: Phase diagrams for effect of alloying elements in titanium	10
Figure 2.4: Process route for obtaining different microstructures: (a) fully lamellar (b) fully equiaxed (c) bi-modal	14
Figure 2.5: Microstructure of two phase titanium alloy: (a) Widmanstatten structure; (b) Basket weave like structure; (c) equiaxed; and (d) duplex	17
Figure 3.1: (a) Vacuum arc melting furnace (b) schematic of vacuum arc melting furnace	30
Figure 3.2: Heat treatment graph	32
Figure 3.3 : Mounted samples for microstructure analysis: (a) before polishing (b) after polishing.....	35
Figure 3.4: Sample for Tensile test: (a) Original sample (b) Sample dimensions in AutoCad.....	37
Figure 3.5: Jigs for tensile testing	37
Figure 3.6: Sample after Rockwell hardness test.....	39
Figure 3.7: Typical surface roughness profile	43
Figure 3.8: Roughness Test Instrument	43
Figure 4.1: Optical micrograph at 50x (a-d) and 100x (e-h) magnifications...	48
Figure 4.2: Tensile test specimen.....	49
Figure 4.3: Stress - strain graph at RT	50
Figure 4.4: Stress-strain curve of lowest Zr content alloy	52
Figure 4.5: Stress-strain curve of highest Zr content alloy	52
Figure 4.6: Ultimate tensile strength values	53
Figure 4.7: Yield strength values	53
Figure 4.8: Rockwell Hardness test results at RT.....	54
Figure 4.9: Volume loss at 8.5 Hz	56
Figure 4.10: Volume loss at 17 Hz	56
Figure 4.11: Wear coefficient v/s load at 8.5 Hz	57

Figure 4.12: Wear coefficient v/s load at 17 Hz	57
Figure 4.13: Optical micrograph before wear test of (a) Sample 1 (b) Sample 2 (c) Sample 3 (d) Sample 4	58
Figure 4.14: Optical micrograph after wear test of (a) Sample 1 (b) Sample 2 (c) Sample 3 (d) Sample 4	58
Figure 4.15: Roughness profile of (a) Sample 1 before wear test (b) Sample 1 (c) Sample 4 after wear test	59
Figure 4.16: DSC Profile	60
Figure 4.17: XRD Result	61

LIST OF TABLES

Table 2.1: Characteristics of Titanium alloy compared to other metals	7
Table 2.2: Summary of commercial and semi-commercial titanium grades and its alloys	12
Table 2.3: β -transus temperature and hot working temperature of some near- α and $\alpha + \beta$ titanium alloys	18
Table 2.4: Basic properties of alloying elements	19
Table 2.5: Temperature range and chemical composition of conventional titanium alloys	21
Table 2.6: Titanium alloys used for airframe	23
Table 3.1: Raw material composition	31
Table 3.2 : Polishing Steps for Optical Microscopy	34
Table 3.3: Etchant Composition	35
Table 4.1: Alloy composition	47
Table 4.2: Tensile test result at room temperature	50
Table 4.3: Tensile properties	51
Table 4.4: Comparison of Tensile strength	55
Table 4.5: Roughness profile parameters	59
Table 4.6: Summary of results	62

NOMENCLATURE

R_a	Average Surface Roughness
R_{max}	Maximum Surface Roughness
R_q	Root Mean Square Roughness
R_t	Maximum Height of the Profile
R_z	Depth of Surface Roughness

ACRONYMS

CFRP	Carbon Fiber Reinforced Plastic
DSC	Differential Scanning Calorimetry
EDM	Electrical Discharge Machining
EDS	Energy Dispersive X-Ray Spectroscopy
HRC	Rockwell Hardness
HT	High Temperature
RT	Room Temperature
UTM	Universal Testing Machine
UTS	Ultimate Tensile Stress
XRD	X-Ray Diffraction
YS	Yield Stress

Chapter 1 INTRODUCTION

In the field of aerospace, mass is almost always the enemy, increasing cost for launch of flight and decreasing vehicle performance. Every kilogram matters in the design. How much weight could be saved in a design if the mass of every fastener on a satellite bus or airplane could be cut in half while still maintaining safety? This is where titanium has found its application for many years now. The demand for expansion of titanium is due to the realization of low fuel consumption by aircrafts possessing titanium alloy. But, titanium usage is strongly limited by its higher cost relative to competing materials like aluminium alloys and steels. Also, various qualifications and high quality management are required for entry into the aerospace industry. Hence, the advantages to using titanium must be balanced against its cost.

In recent years, as carbon fiber reinforced polymer (CFRP) has come to the forefront, titanium alloys with physical characteristics similar to those of CFRP materials have become more commonly used. Airframe maintenance costs can be effectively reduced through the use of materials excellent in fatigue strength, crack propagation resistance, fracture toughness, and corrosion resistance. Steel based materials were used for portions where high strength was required (frames and joints). Nowadays, titanium alloys are widely used in those places due to their light weight density (density being 60% as that of steel), high strength and excellent corrosion resistance. The demand for titanium is growing. These days, numerous titanium alloys are used for aircraft frames as well as in aircraft engines.

Turbo fan engines are widely employed by commercial aircraft to improve combustion efficiency, and thereby improve fuel consumption. Fuel combustion in the rear section of the engine runs the gas turbine and fan blades in the fore section. Propulsion thrust is generated by the reaction force of the rearward flow of air taken in from the front by the blades, and the rearward

discharge of combustion gases. Turbo fan engines of this type consist of four sections. They are, in order from the front: the fan, compressor, combustion chamber, and turbine. A titanium alloy is mainly used for the fan and the compressor in the fore half section, where the temperature is relatively low (600°C or lower). For the turbine and the combustion chamber in the rear half section where temperatures are higher, nickel-based or iron-based alloys are used [1]. Ti-6Al-4V, Ti-6Al-2Sn-4Zr-6Mo, Ti-3Al-8V-6Cr-4Zr-4Mo, Ti-5Al-2.5Sn (IMI 317) and Ti-6Al-5Zr-0.5Mo-0.25Si (IMI 685) are some of the currently used commercial titanium alloys in the aerospace industry.

This thesis aims to investigate the effect of zirconium addition on the strength of titanium, and to produce a high strength titanium alloy by vacuum arc melting process and subsequent heat treatment following it. The effect of increase in zirconium content on titanium alloys have not yet been studied thoroughly. In this study, titanium alloy with four different alloy compositions are investigated upon. The alloys were prepared by vacuum arc re-melting and heat treatment following it. Then the alloys were cut in to required geometry by wire-EDM cutting. The microstructural effects were studied by optical microscopy. Various mechanical properties like tensile strength, yield strength, hardness, wear rate and surface roughness were found out. The β -transus temperature was studied upon. XRD analysis was used to identify the phases formed in the alloys.

Zr is chosen in this study because it has the same crystal structure as titanium (hcp) at room temperature. Also, Zr is completely soluble and a good solid solution strengthener in Ti. Therefore, desirable mechanical properties may be obtained by optimising the alloy composition and the thermo-mechanical processing methods [2].

1.1 Organization of the Thesis

Chapter 1 gives a brief outline of this thesis, and how the report has been organized.

Chapter 2 introduces the field of titanium and its alloys. The past research works done on this topic are also reviewed. Then the objective of this study is stated.

Chapter 3 introduces the various techniques used in this project, which include both synthesis and characterization techniques employed to study the mechanical and microstructural properties of the alloys.

Chapter 4 discusses the results in detail obtained from tensile, hardness, wear, roughness, XRD and DSC tests. It also explains the limitations faced with during the course of the study.

Chapter 5 finally gives the conclusion of the work in this thesis.

A flowchart representing the research methodology in thesis is shown below (Figure 1.1).

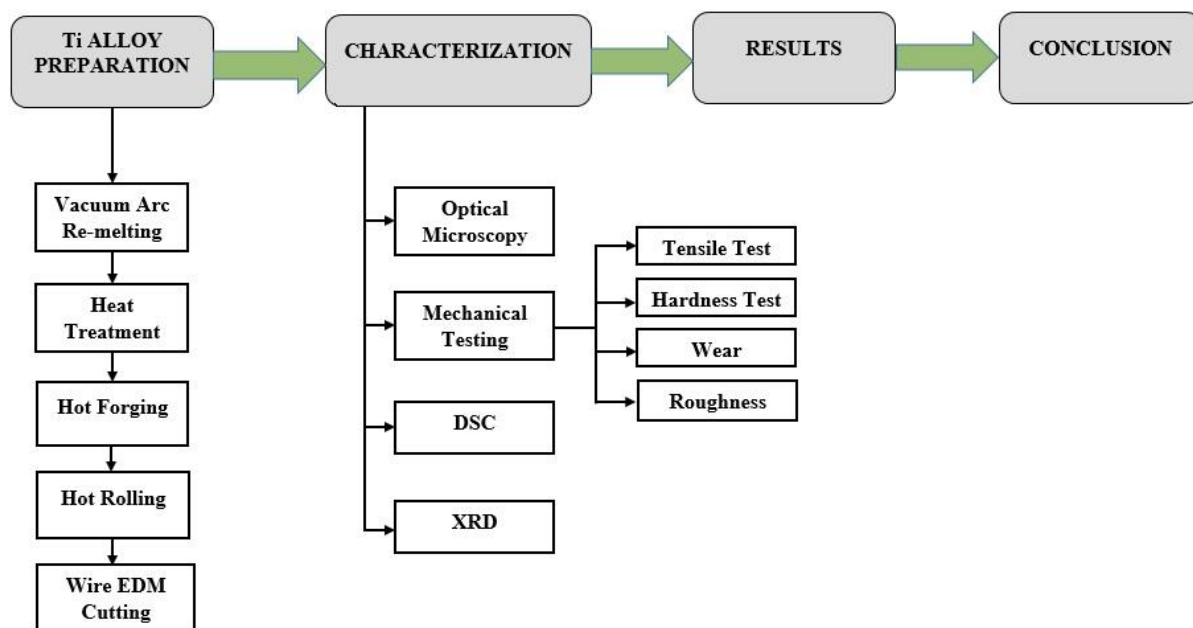


Figure 1.1: Research Methodology

Chapter 2 LITERATURE REVIEW

2.1 Introduction to Titanium

Titanium (Ti) is a chemical element with atomic weight 47.867 amu and atomic number 22. It is a lustrous transition metal with a silver colour, low density (4510 kg/m^3) and good strength. It is nonmagnetic, and transfers heat well. Its melting point is 1993 K ($1668 \text{ }^\circ\text{C}$). There are two allotropic forms and five naturally occurring isotopes of this element: ^{46}Ti , ^{47}Ti , ^{48}Ti , ^{49}Ti and ^{50}Ti , with ^{48}Ti being the most abundant (73.8%).

Titanium was discovered in Cornwall, Great Britain by William Gregor in 1791, and was named by Martin Heinrich Klaproth after the Titans of Greek mythology. The use of titanium metal, in any form, only really developed after World War II. In fact, titanium was not isolated as a metal until the American chemist Matthew Hunter produced it by reducing titanium tetrachloride (TiCl_4) with sodium in 1910; a method now known as the Hunter process. Commercial production, however, did not come until after William Justin Kroll showed that titanium could also be reduced from chloride using magnesium in the 1930s. The Kroll process remains the most important commercial production method to this day. After a cost-effective production method was developed, titanium's first major use was in military aircraft. Both Soviet and American military aircraft and submarines designed in the 1950s and 1960s began making use of titanium alloys. By the early 1960s, titanium alloys started to be used by commercial aircraft manufacturers as well.

The element occurs within a number of mineral deposits, principally rutile (TiO_2) and ilmenite (FeTiO_3), which are widely distributed in the Earth's crust and lithosphere, and it is found in almost all living things, water bodies, rocks, and soils. The metal is extracted from its principal mineral ores by the Kroll and Hunter process. Titanium's most common compound, titanium dioxide (TiO_2), is a popular photo-catalyst and is used in the manufacture of white pigments. Other compounds include titanium tetrachloride (TiCl_4), a component of smoke screens and catalysts; and titanium trichloride (TiCl_3),

which is used as a catalyst in the production of polypropylene [3]. Due to its corrosion resistance and high strength-to-density ratio (the highest of any metallic element), titanium finds its use in plenty of fields.

The crystal structure of titanium at ambient temperature and pressure is close packed hexagonal α phase with c/a ratio of 1.587 (Figure 2.1-a). However, at 882.5 °C, titanium undergoes an allotropic transformation to a body centred cubic β phase (Figure 2.1-b), which remains stable up to the melting temperature of 1668 °C.

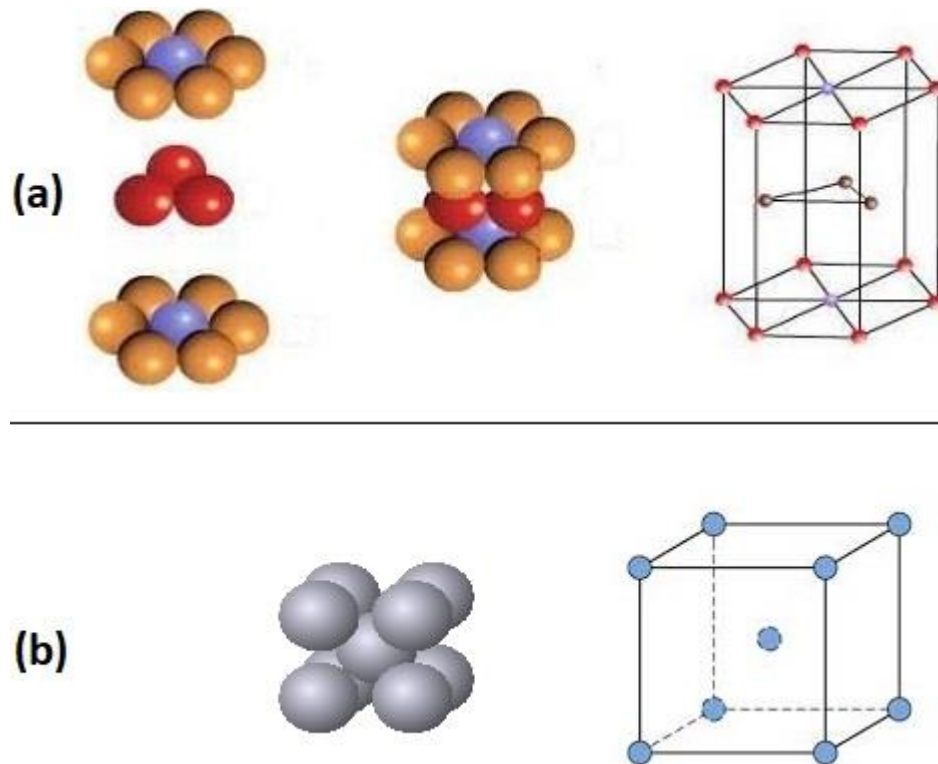


Figure 2.1: Ti crystal structure (a) hcp (b) bcc

The advantages of titanium are notable. It combines the high melting point of iron and nickel and the superior corrosion resistance (room temperature) and density of aluminium. Furthermore, its strength is modest, and like iron, it is capable of strengthening by allotropic transformation.

2.2 Alloying of Titanium

Titanium can be alloyed with iron, aluminium, vanadium, molybdenum, etc. to produce strong, lightweight alloys for aerospace (jet engines and spacecraft), military (missiles), industrial processes, automotive, medical prostheses, orthopaedic implants, dental and endodontic instruments and files, sporting goods, and other applications. This is due to their unique merits of low density, high specific strength, heat resistance, corrosion resistance, low temperature resistance, and excellent biocompatibility. In its unalloyed condition, titanium is as strong as some steels, but less dense. Table 2.1 shows the general characteristics of titanium and its alloys as compared to other important structural metallic materials such as Fe, Al and Ni, which are already widely used.

Table 2.1: Characteristics of Titanium alloy compared to other metals

Material Property	Ti	Fe	Ni	Al
Melting Temperature (°C)	1670	1538	1455	660
Allotropic Transformation (°C)	$\beta \xrightarrow{882} \alpha$	$\gamma \xrightarrow{912} \alpha$	-	-
Crystal Structure	bcc \rightarrow hex	fcc \rightarrow bcc	fcc	fcc
Yield Stress Level (MPa)	1000	1000	1000	500
Density (g/cm ³)	4.5	7.9	8.9	2.7
Corrosion Resistance	very high	low	medium	high
Reactivity with Oxygen	very high	low	low	high
Comparative price of metal	very high	low	high	medium

Ti-6Al-4V (Ti-64) is the most widely used of all titanium alloys since it can be heat-treated to various levels and is comparatively easy to be machined. The attainment of long lasting metal-metal bonds utilizing titanium adherents has been an important area of concern, particularly for aerospace and defence industries. Therefore based on this concern, most research into the effects of the surface-treatment of the adherent has been carried out by these specific industries.

However, applications of titanium and titanium alloys are limited by many of the shortcomings in titanium itself, such as a low elastic modulus compared with ferrous alloys, low heat conductivity, more difficult to plastically deform compared with other engineering alloys, poor oxidation resistance at high temperature, low wear resistance and a high friction coefficient. So to overcome these drawbacks, the development of titanium matrix composites and titanium based alloys with high performance have become more and more important research topics.

Solid solution strengthening is a type of alloying that can be used to improve the strength of a pure metal. The technique works by adding atoms of one element (the alloying element) to the crystalline lattice of another element (the base metal), to form a solid solution. This results in either substitutional (Figure 2.2 a&b) or interstitial point defects (Figure 2.2-c) in the crystal [4]. The local non-uniformity in the lattice due to the alloying element makes plastic deformation more difficult by impeding dislocation motion.

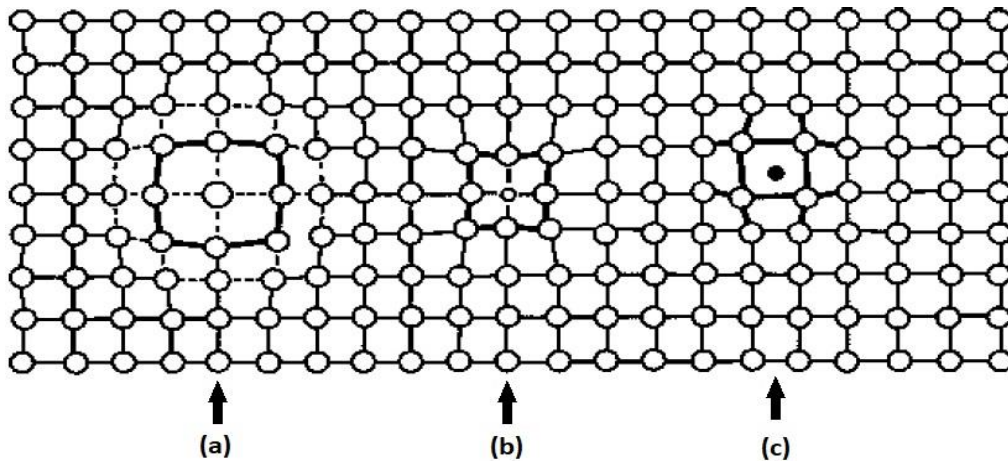


Figure 2.2: Schematic for solid solution strengthening with (a) small (b) large substitutional atoms; and (c) interstitial atoms

The strength of a material is dependent on how easily dislocations in its crystal lattice can be propagated. The dislocations create stress fields within the material depending on their character. When solute atoms are introduced, local stress fields are formed that interact with those of the dislocations, causing the solute atoms to act as potential barriers, impeding their motion and causing an

increase in the yield stress of the material, which means an increase in strength of the material. This gain is a result of both lattice distortion and the modulus effect. Surface carburizing, or case hardening, is an example of solid solution strengthening in which the density of solute carbon atoms is increased close to the surface of the steel, resulting in a gradient of carbon atoms throughout the material. This provides superior mechanical properties to the surface of the steel without having to use a higher-cost material for the component. Strengthening by heat treatment is also possible.

2.3 Classification of Titanium alloys

According to different alloying additions and phases present in the microstructures, titanium alloys are classified conventionally into three categories:

- α alloy;
- $\alpha + \beta$ alloy; and
- β alloy (which can be further divided into stable β and metastable β alloys).

The processing and behaviour of titanium and its alloys is strongly dependent on two allotropic forms of titanium: the α phase, with a hexagonal close-packed structure, exists from room temperature to 882°C for pure titanium. Some elements dissolve preferentially in the α phase and are α stabilisers. The α phase field is therefore expanded with an increase in the α/β transus temperature. Typical α stabilisers are Al, O, N etc. The β phase, which is a body-centred cubic structure, exists from 882°C to the melting point for pure titanium. Some elements depress the α/β transus promoting β phase retention when cooling from the single β phase. Elements which are β stabilisers are Mo, V, Nb, Fe, H, etc. [5] These transformations enable titanium to have alloys designated as α , β or α/β with various microstructures and specific properties.

Figure 2.3 schematically shows the phase diagrams of the effect of alloying addition in titanium alloy. Aluminium (Al), oxygen (O), nitrogen (N) and carbon (C) are all strong α -stabilizers. These elements can increase the β -transus temperature with increasing solute contents, as shown in Figure 2.1 (a). Aluminium is the most widely used alloying element in titanium alloys, because it can increase the transus temperature and lead to strengthening effect due to large solubility in both α and β phases. Oxygen is sometimes used to obtain a desirable strength via solid solution strengthening effect, but nitrogen and carbon are usually impurities.

The β -stabilizing elements are actually divided into β -isomorphous elements and β -eutectoid forming elements depending on different binary phase diagrams. These two kinds of phase diagrams are shown schematically in Figure 2.1 (b) and 2.1 (c). Molybdenum (Mo), Vanadium (V), Niobium (Nb) and Tantalum (Ta) are the most widely used isomorphous ones. But, chromium (Cr), iron (Fe), copper (Cu) and silicon (Si) belong to the eutectoid elements.

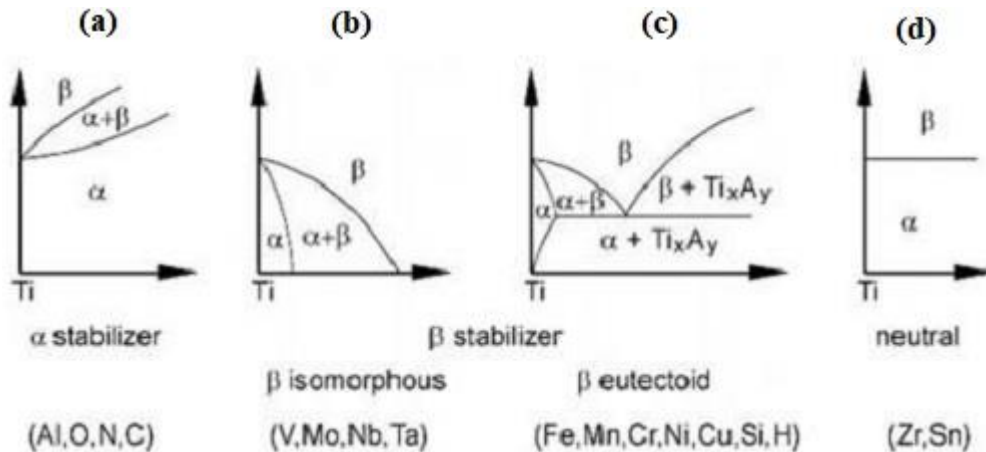


Figure 2.3: Phase diagrams for effect of alloying elements in titanium

Additionally, there are other elements like zirconium (Zr), hafnium (Hf) and tin (Sn) called neutral elements because of their very slight influence on the transformation temperature.

Table 2.2 shows some of the main commercial and semi-commercial titanium alloys used in various industries today [6]. The table displays examples of unalloyed titanium grades, α alloys, near- α alloys, $\alpha+\beta$ alloys and β alloys.

2.3.1 α alloys

Depending on the cooling rates, the microstructure can be composed of equiaxed α , Widmanstätten lath-like α phase or martensitic α' phases. These alloys are non-heat treatable alloys, having moderate strength, good toughness, superior high temperature creep, oxidation resistance and weldability [7]. The α alloys can tolerate a small amount of β phase (2-5%) upon cooling from the α phase field, which are called near- α alloys. The small amount of β phase in the near- α alloys is useful for better controlling the recrystallized α grain size and improving mechanical properties. Compared to pure titanium with different grades, the near- α alloys exhibit some advantages like improved tensile strength, workability and heat treatability, which broaden the application of α alloys [8]. α phase stabilizing elements include aluminium, tin, zirconium and oxygen. These alloying elements give significant rise to solid solution hardening, thereby increasing tensile strengths by 35 – 70 MPa per percent of element added [9].

2.3.2 $\alpha+\beta$ alloys

The group of $\alpha+\beta$ alloys contains a limited quantity of α -stabilizers and β -stabilizers. The addition of α -stabilizer is used to strengthen the α phase, while β -stabilizers allow the β phase to be retained at room temperature after cooling from β or $\alpha + \beta$ phase fields. The most used $\alpha + \beta$ alloy is the Ti-6Al-4V alloy containing 15 vol. % of β phase in equilibrium at 800°C.

The mechanical properties of $\alpha+\beta$ alloys depend on the relative amount and distribution of α and β phases [10]. These variables are controlled by appropriate heat treatment and/or thermo-mechanical processing. Heat treatment consisting of a quench from a temperature in the alpha-beta range,

followed by an ageing cycle at a reduced temperature can significantly strengthen the $\alpha+\beta$ alloy. Even though heat-treated alpha-beta alloys are stronger than the alpha alloys, their ductility is proportionally lower [11].

Table 2.2: Summary of commercial and semi-commercial titanium grades and its alloys

Alloy	Yield strength (MPa)	Tensile strength (MPa)	Chemical composition (wt %)					
			Al	Sn	Zr	Mo	V	Others
Unalloyed grades								
ASTM Gr.1	170	240	-	-	-	-	-	-
ASTM Gr.2	280	340	-	-	-	-	-	-
ASTM Gr.3	380	450	-	-	-	-	-	-
ASTM Gr.4	480	550	-	-	-	-	-	-
ASTM Gr.7	280	340	-	-	-	-	-	0.2 Pd
α and near-α alloys								
Ti-0.3Mo-0.8Ni	380	480	-	-	-	0.3	-	0.8 Ni
Ti-5Al-2.5Sn	760	790	5	2.5	-	-	-	-
Ti-5Al-2.5Sn-ELI	620	690	5	2.5	-	-	-	-
Ti-8Al-1Mo-1V	830	900	8	-	-	1	1	
Ti-6Al-2Sn-4Zr-2Mo	830	900	6	2	4	2	-	-
Ti-6Al-2Nb-1Ta-0.8Mo	690	790	6	-	-	1	-	2 Nb, 1Ta
Ti-2.25Al-Sn-5Zr-1Mo	900	1000	2.25	11	5	1	-	0.2 Si
Ti-5Al-5Sn-2Zr-2Mo	830	900	5	5	2	2	-	0.25 Si

$\alpha+\beta$ alloys								
Ti-6Al-4V	830	900	6	-	-	-	4	
Ti-6Al-4V- ELI	760	830	6	-	-	-	4	
Ti-6Al-6V- 2Sn	970	1030	6	2	-	-	6	0.75 Cu
Ti-8Mn	760	860	-	-	-	-	-	8 Mn
Ti-7Al-4Mo	970	1030	7	-	-	4	-	-
Ti-6Al-2Sn- 4Zr-6Mo	1100	1170	6	2	4	6	-	-
Ti-5Al-2Sn- 2Zr-4Mo-4Cr	1055	1125	5	2	2	4	-	4 Cr
Ti-6Al-2Sn- 2Zr-2Mo-2Cr	970	1030	5.7	2	2	2	-	2 Cr, 0.25 Si
Ti-3Al-2.5V	520	620	3	-	-	-	2.5	
β alloys								
Ti-3Al-10V- 2Fe	1100	1170	3	-	-	-	10	
Ti-3Al-13V- 11Cr	1100	1170	3	-	-	-	13	11 Cr
Ti-3Al-8V- 8Mo-2Fe	1100	1170	3	-	-	8	8	
Ti-3Al-4Zr- 8V-4Mo-6Cr	830	900	3	-	4	4	8	6 Cr
Ti-6Zr-4.5Sn- 11.5Mo	620	690	-	4.5	6	11.5	-	-

In terms of microstructure, there can be fully lamellar structures, fully equiaxed structures or bi-modal microstructures. These different microstructures are obtained through a certain process route shown in Figure 2.4. For fully lamellar microstructures shown in Figure 2.4(a), after the first step (homogenization) above β transus, the deformation process can be done by

forging or rolling, either in the β phase field or in the $\alpha+\beta$ phase field. The third step (recrystallization) is usually kept at a temperature slightly higher than the β transus to control the β grain size. The cooling rate from the β phase field after recrystallization is a crucial parameter determining the width of the α -lamellae. The final step (annealing) is a stabilization treatment that aims essentially to form an equilibrium structure, such as fully developed secondary α plates.

The fully equiaxed structure shown in Figure 2.4(b), can be obtained through two methods. The first one is the same process route for obtaining the bi-modal microstructure; the only difference is the final step extended until the equiaxed primary α grains stops growing and forms triple-points. The other method for developing the fully equiaxed microstructure is to decrease the recrystallization temperature in order to obtain high volume fraction of α phase.

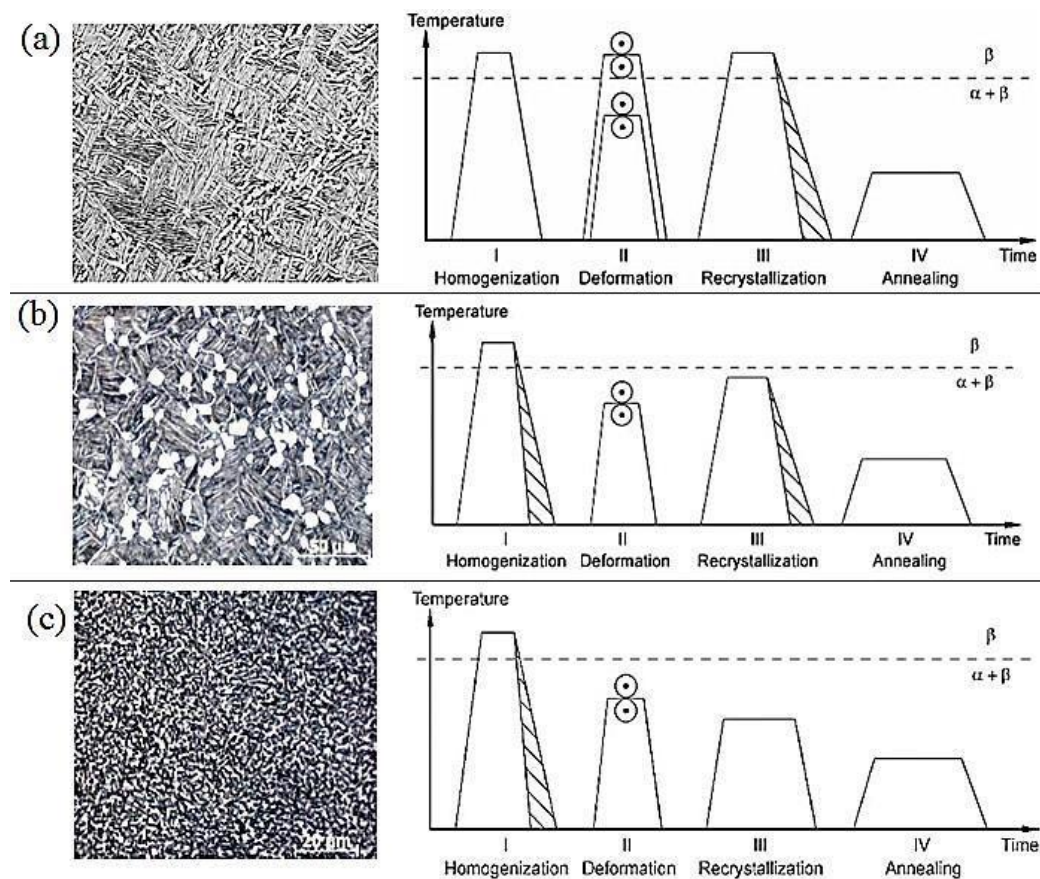


Figure 2.4: Process route for obtaining different microstructures: (a) fully lamellar (b) fully equiaxed (c) bi-modal

The bi-modal microstructure is shown in Figure 2.4(c). The process route is divided into four steps: homogenization in the β phase field, deformation in the $\alpha+\beta$ phase field, recrystallization in the $\alpha+\beta$ phase field and finally annealing treatment for stress removing and grain growth.

Generally speaking, the two phase $\alpha+\beta$ alloys offer a wide range of combinations of strength, toughness and high temperature properties that makes them attractive in wide ranging aerospace and other fields demanding high specific properties to temperature of about 600 °C.

2.3.3 β alloys

When sufficient β stabilizing elements are added into titanium, β alloys can be produced. The β -stabilizing elements include vanadium, molybdenum, niobium and tantalum [12]. Ti-15V-3Cr-3Sn-3Al (Ti-15-3) is the most widely used beta titanium alloy due to its high strength-to-weight ratio, good cold formability and excellent corrosion resistance [13]. Actually, the β alloys include stable β alloys and metastable β alloys. In Figure 2.4, the metastable β alloys lie in the equilibrium $\alpha+\beta$ region of the phase diagram and stable β alloys locates in the β single phase field.

- **Stable β alloys**

If more content of β -stabilizing elements is added into titanium, the β -transus temperature can be decreased below room temperature. After cooling to room temperature, stable β alloys can be formed. It is not surprising that the percentage of β alloys is now steadily increasing due to the attractive properties, such as heat treatability, wide and unique range of strength/weight ratios, deep hardening potential and inherent ductility. In addition, they possess superior fatigue resistance as compared to $\alpha+\beta$ alloys. These alloys can be predicted to appear in aerospace, power plant, sporting goods, automotive and biomedical health applications.

- **Metastable β alloys**

The metastable β alloys are characterized by non-martensitic transformation upon fast cooling from the β phase field. In another words, the metastable β phase can be retained to room temperature by quenching from the β phase field. However, α phase can precipitated from the metastable β phases as very fine size in the subsequent annealing process below β -transus temperature, resulting in much higher yield stress levels. This type of β alloys is generally more easily cold workable than the $\alpha + \beta$ alloys, heat treatable and has good corrosion resistance. Therefore, it is not surprising that the application of metastable β alloys has been slowly increasing in recent years [14].

In titanium, the alloying elements stabilises the alloy to either low temperature close packed hexagonal α phase, or the high temperature body centred cubic β phase. The conventional titanium alloys used in aerospace applications contain both the α phase and the β phase stabilising elements in proportions suitable for the application in hand. The α phase, because of its hcp structure, exhibits lower value of diffusivities than the bcc structured β phase. Thus, the α phased alloys forms a major constituent ($> 95\%$) in high temperature titanium alloys.

There are four main kinds of microstructure found in a two phase titanium alloy: A Widmanstatten structure (fully lamellar), a basket-weave like structure (fully lamellar), an equiaxed structure and a duplex microstructure as shown in Figure 2.5.

The main characteristics of Widmanstatten structure are coarse primary β grains, a continuous α phase along the grain boundaries, a lamellar α phase within the prior β grains and a β phase between the α lamellae. The Widmanstatten microstructure is always formed when both the starting and finishing temperatures during deformation remain within a single phase region. The cooling rate determines the final morphology of the α phase: fine lamellae are always obtained at faster cooling rates while coarser lamellae are obtained at lower cooling rates. A two phase alloy with a Widmanstatten structure always

exhibits a relatively high tensile strength at room temperature but with low ductility. The ductility and fatigue properties given by an alloy with a basket-weave type of microstructure are always better than those found in material with a Widmanstatten microstructure. However, the fracture toughness is always lower than that found in material with a Widmanstatten structure.

An equiaxed microstructure always gives better ductility but lower strength and fracture toughness compared with the other three type of microstructure. So, different processing methods are applied to produce different kinds of microstructure which directly affect the mechanical properties of a two phase titanium alloy. A clear understanding of microstructure development and the relationship between microstructure and mechanical properties is very important for designing the processing parameters for titanium alloys.

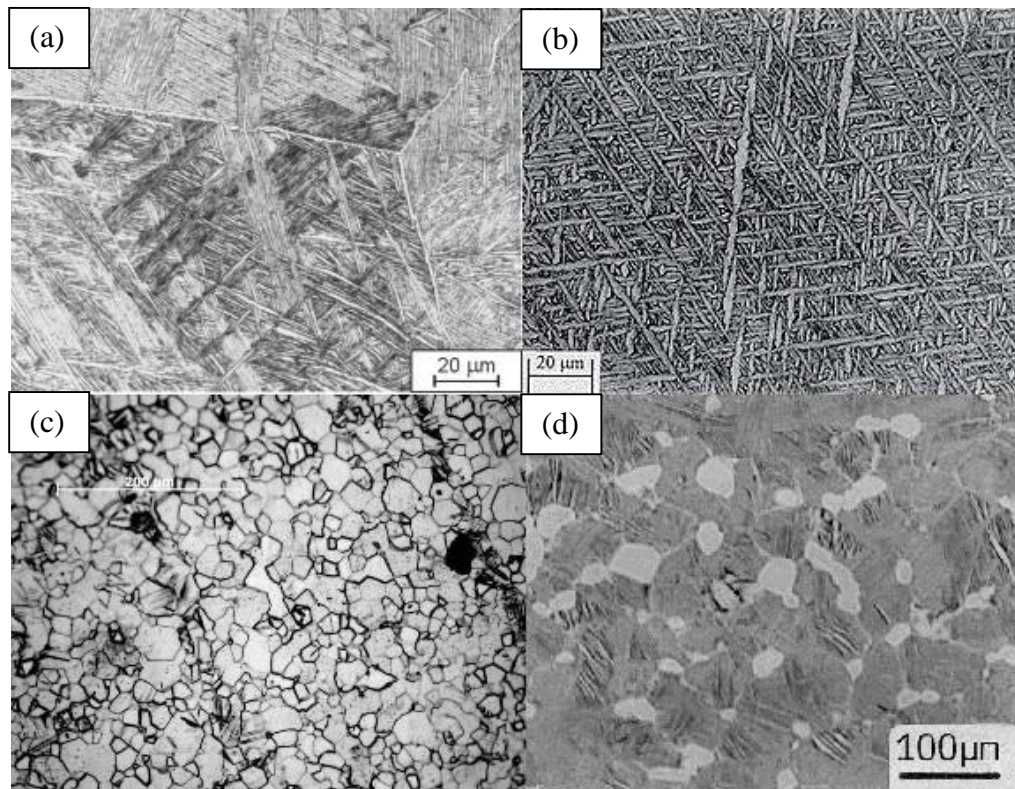


Figure 2.5: Microstructure of two phase titanium alloy: (a) Widmanstatten structure [15]; (b) Basket weave like structure [16]; (c) equiaxed; and (d) duplex [17]

The recommended working temperatures for some near- α and $\alpha+\beta$ alloys are shown in Table 2.3 . The working temperature has been designed for the alloy to meet specific requirements with respect to the application it is being used for.

Table 2.3: β -transus temperature and hot working temperature of some near- α and $\alpha+\beta$ titanium alloys

Alloy	β-transus temperature (°C)	Secondary hot working temperature (°C)
Ti-5Al-2.5Sn	1040	900-1010
Ti-8Al-1Mo-1V	1040	900-1010
Ti-6Al-4V	995	860-980
Ti-6Al-2Sn-4Zr-2Mo	990	920-975
Ti-6Al-2Sn-2Zr-2Mo-2Cr	980	870-955
Ti-6Al-6V-2Sn	945	845-915
Ti-6Al-2Sn-4Zr-6Mo	940	850-910
Ti-4.5Al-5Mo-1.5Cr	925	850-910
Ti-17 (Ti-5Al-2Sn-2Zr-4Cr-4Mo)	885	800-865

In this study, titanium is alloyed with zirconium, aluminium, tin, molybdenum, niobium and silicon. Except for zirconium, the compositions of all the other elements were maintained constant. Aluminium is the prime α stabilizer. Molybdenum, niobium and silicon are the β stabilizers. Finally, tin and zirconium are the neutral stabilizers. The amount of β elements is very low, but sufficient enough to confer some microstructural strengthening without endangering mechanical stability. Table 2.4 lists some properties of the elements used in this study.

Table 2.4: Basic properties of alloying elements

Element	Atomic number	Atomic mass (amu)	Density (g/cm ³)	Melting point (°C)	Crystal structure at RT
Titanium (Ti)	22	47.867	4.506	1668	hcp
Aluminium (Al)	13	26.982	2.7	660.32	fcc
Zirconium (Zr)	40	91.224	6.52	1855	hcp
Tin (Sn)	50	118.71	7.31	231.93	tetragonal
Molybdenum (Mo)	42	95.95	10.22	2623	bcc
Niobium (Nb)	41	92.906	8.57	2477	bcc
Vanadium (V)	23	50.942	6.0	1910	bcc

Aluminium (Al) is an α -stabilizer with significant solid solubility. Aluminium replaces atoms from the titanium matrix substantially. The addition of aluminium to titanium increases its tensile strength and creep strength, while decreasing the alloy density. Presence of aluminium retards the rate of transformation to the β phase. However, the addition of aluminium above 7% leads to formation of titanium aluminide (Ti_3Al) precipitates [18]. Empirical testing has brought up the Al-equivalent equation given below. It ensures an α -alloy is obtained as long the Al-equivalent does not exceed 9% [5, 19].

$$Al_{eq} = 1 Al + \frac{1}{3} Sn + \frac{1}{6} Zr + 100 < 9\%$$

Zirconium (Zr) forms a continuous solid solution with titanium, and increases the strength of the alloy at low and intermediate temperatures. Unlike aluminium and tin, zirconium is fully soluble in titanium. But, the addition of

zirconium above 5 – 6 % reduces the alloys' creep strength along with its ductility, and decreases the transus temperature slightly [20]. The oxidation behaviour in air becomes dramatically worse with zirconium addition and leads to rapid ZrO₂ formation at temperatures above 600°C.

Tin (Sn) is often used in conjunction with aluminium to give higher strength to the alloy without embrittlement. But, the alloy density may be compromised with the addition of tin. Tin is a weak β -stabilizer. So it delays the rate of transformation to the β phase. Together with aluminium, tin behaves as an α -stabilizer [21]. Tin is like zirconium, classically considered as a neutral element in terms of phase stability [5]. Tin is also found to be a good solid solution strengthener in titanium.

Molybdenum (Mo) is the prime β stabilizer being used here. Molybdenum increases the heat treatment response of the alloy as well as the strength at high temperatures for a short time, but materials containing high Mo content are difficult to weld. Also in long term, molybdenum decreases the creep strength. Mo mainly finds its place in applications where high strength is required for short time, or where superior strength is required at low temperatures.

Niobium (Nb) is another β stabilizer used. It improves the surface stability and strength of the alloy at high temperature. It can also provide good corrosion resistance during high temperature exposure. Sometimes, niobium is substituted for some amount of molybdenum to provide β phase strengthening with the least possible lowering of the β transus temperature of the alloy.

Silicon (Si) is a β stabilizing element, which is very important element in the alloying addition of high temperature titanium alloys, because it increases the strength of the alloy at all temperatures, and has a marked beneficial effect on creep resistance and oxidation resistance. But, the presence of silicon above 0.5 % decreases the ductility, and also leads to formation of silicides with zirconium, which leads to embrittlement of the alloy.

Table 2.5 lists the temperature range and chemical composition of some conventional titanium alloys made from the elements in this discussion [22]. It is a combination of α alloys, $\alpha+\beta$ alloys and β alloys. The alloy composition has been selected in such a way that it serves the purpose of the application it has been designed for.

Table 2.5: Temperature range and chemical composition of conventional titanium alloys

Alloy	Max Useful Temperature (°C)	Chemical Composition (wt %)							
		Al	Sn	Zr	Mo	Nb	V	Si	Others
IMI 318	300	6	-	-	-	-	4	-	-
IMI 550	425	4	2	-	4	-	-	0.5	-
Ti-811	400	8	-	-	1	-	1	-	-
IMI 679	450	2	11	5	1	-	-	0.2	-
Ti-6246	450	6	2	4	6	-	-	-	-
Ti-6242	450	6	2	4	2	-	-	-	-
IMI 685	520	6	-	5	0.5	-	-	0.5	-
Ti-6242S	520	6	2	4	2	-	-	0.1	-
IMI 829	580	5.5	3.5	3	0.3	1	-	0.3	-
IMI 834	590	5.5	4	4	0.3	1	-	0.5	0.06 C
Ti-1100	600	6	2.8	4	0.4	-	-	0.4	-
VT3-1	-	6.5	-	-	2.7	-	-	0.25	1.6 Cr
VT 9	520	6.5	-	2	3.5	-	-	0.25	-
VT 18	-	6	-	11	1	1	-	0.1	-
VT 18Y	550	6.9	2.7	4.1	0.9	1	-	0.15	-
Ti-633G	-	5.5	3	3	0.3	1	-	0.3	0.2 Gd
Ti-55	-	5.5	4	2	1	-	-	0.25	1 Nd
DAT 54	550	5.8	4	3.5	2.8	0.7	-	0.4	0.06 C

2.4 Titanium in Aerospace

Nowadays, titanium and its alloys are becoming increasingly attractive for a wide range of applications in many fields such as military and civil transportation. The development of supersonic military aircrafts after World War II necessitated an intensive research effort to develop new structural alloys which could withstand the demanding operational conditions of both airframes and gas turbine engines. Titanium has exceptional properties of strength, specific strength, low-thermal expansion coupled with low modulus in relation to its high-low cycle fatigue strength, corrosion resistance, workability, and weldability. The class of titanium alloys based on near-alpha compositions, could lead to compressor sections of future advanced commercial engines built almost entirely from titanium alloys. No other material approaches this combination of engineering properties over a temperature range spanning from ambient temperature to about 550 °C. Accordingly, this single material has been dominant in aero engine application in the compressor stages. It is noted that the aluminium and steel used for the earliest aero engines have been succeeded almost entirely in today's advanced military and civil aircraft engines by titanium base alloys and nickel base alloys. The use of titanium alloys in the present day aero engines has made it possible to bring out further improvements in aerodynamic component, cycle and propulsive efficiency coupled with improvements in thrust-to-weight ratio.

Increased use of titanium in hotter sections of gas turbine engines is usually at the expense of nickel-based alloys. Further work in the area of alloy development, process optimization, and improved oxidation resistance can lead to an additional increase of the temperature range, allowing use of these alloys in the low-pressure turbine section of gas turbine engines for increased efficiency.

The weight of jet engines in modern aircrafts can be reduced considerably through substitution of heavy nickel base alloys in the compressor part of the turbines by suitable less dense high strength titanium alloys. Thus,

the payload can be increased and the consumption of fuel is reduced. The most recent high-temperature titanium alloy IMI 834 (Ti-5.68Al-4Sn-3.5Zr-0.6Nb-0.5Mo-0.3Si) was developed for using as discs and blades, combines good creep and fatigue properties up to the intended service temperature of 600°C. Some of the conventional titanium alloys used for aircraft frames currently are mentioned in Table 2.6.

Table 2.6: Titanium alloys used for airframe

Alloy	Application
Ti-6Al-4V	Cockpit window frame, wing box, fastener
Ti-3Al-2.5V	Hydraulic pipe
Ti-10V-2Fe-3Al	Landing gear, tracking beam
Ti-6Al-2Sn-4Zr-2Mo	Exhaust, tail cone
Ti-15V-3Cr-3Sn-3Al	Duct

For aircraft engines, titanium alloys stronger than pure titanium are used for their light weight, high strength (high specific strength) and heat resistance properties. Aluminium alloys with high specific strength are rarely used in aircraft engines because their strength drops sharply at temperatures of about 200°C and above. Although the specific strength of titanium alloys deteriorates as the temperature rises, their specific strength is superior to that of Ni-based alloy in the temperature range between 500 – 600 °C.

Previous studies have shown that the Ti-Al-Mo-V alloy has good strength, but the plasticity is poor. Ti-6Al-4V is one of the titanium alloys used for aircraft engines at present. The demand for titanium for airframes and engines is increasing, accompanied by improvements in aircraft fuel consumption. Various titanium materials are used, each material carefully selected according to the specific use. Some of the commonly used titanium alloys for aircraft engines are as follows:

1) **Ti-6Al-2Sn-4Zr-2Mo alloy**

Ti-6Al-2Sn-4Zr-2Mo alloy is a heat resistant alloy developed in the latter half of 1960s. Its heat resistant temperature is approximately 450°C. later in the 1970s, Ti-6Al-2Sn-4Zr-2Mo-0.1Si was developed to improve oxidation resistance and creep property with the addition of Si of 0.06~0.2wt%, and the heat resistant temperature was improved to approximately 500°C. Therefore, this alloy is commonly used for compressor discs where 500°C is the upper service temperature limit. The yield strength of annealed material of the alloy is 860 MPa with a tensile strength of 930 MPa, and elongation of 10% at room temperature [23]. As the alloy has less β phase than Ti-6Al-4V alloy, ageing treatment is not effective. Therefore, the alloy is normally used after solution heat treatment, at a temperature at least 35°C below the β transformation temperature, followed by stabilizing annealing for about 8 hours at 590°C.

2) **Ti-8Al-1Mo-1V alloy**

Ti-8Al-1Mo-1V alloy was developed in the 1960s. Its heat resistant temperature is approximately 400°C. It is used for compressor blades rather than fan blades. The yield strength of the annealed material is 930 MPa with a tensile strength above 1000 MPa, and elongation of 10% at room temperature. Similar to Ti-6Al-2Sn-4Zr-2Mo-0.1Si, this alloy has less β phase and is therefore used after solution heat treatment and stabilizing annealing.

3) **Ti-5Al-2Sn-2Zr-4Cr-4Mo (Ti-17) alloy**

Ti-5Al-2Sn-2Zr-4Cr-4Mo alloy, commonly referred to as Ti-17 alloy was developed in the USA in the 1970s as an alloy having high strength and excellent fracture toughness. Its heat resistant temperature is approximately 350°C. In commercial aircraft engines, the fan and shaft are built as one piece to reduce engine weight. The yield strength and tensile strength at room temperature are 1150 MPa and about 1250 MPa respectively, higher than those of Ti-6Al-4V alloy by about 200 MPa.

The alloy exhibits excellent crack propagation characteristics, and is appropriate for damage tolerance design.

2.5 Titanium as Biomaterials

Titanium and titanium based alloys are commonly used biomaterials for transcutaneous implants because of their mechanical strength, biocompatibility, non-toxicity, corrosion resistance and ease of processability. These materials are used in a large range of clinical devices such as prostheses, craniofacial and dental implants [24].

Studies on surface treatments of titanium are in progress to increase the adhesion of bone tissue and implants. It is clear that any reduction in ion release will prove to be beneficial for the patient and may increase implant lifetime, thereby avoiding the need for re-surgery [25]. This is mostly true for a porous and cement-less implant wherein a large surface area of the implant is exposed to the bio-environment. When an implant is placed in a physiological environment, metal ions are released which could cause local and systemic effects [26]. Ti-6Al-4V is an inert implant material with excellent mechanical properties. In the case of the alloy, titanium ions accumulate in local tissues after long periods of time giving rise to dark tissue staining with unknown consequences. The corrosion resistance of Ti-6Al-4V alloys are mainly due to their ability to form a stable passive film, which rapidly forms on the alloy and provides a barrier between the bio-environment and alloy substrate. Previous works have reported that modification of the surface oxide may reduce the metal ion dissolution into saline solution [27]. Although the healing time becomes extended with the use of titanium alloys, the chemical combination of the metal with bone is known to decrease the active induction of bone formation.

Osseointegration is defined as the formation of a direct interface between an implant and bone, without intervening soft tissue. Osseo integrated implant is a type of implant defined as an endosteum implant containing pores

into which osteoblasts and supporting connective tissue can migrate. Applied to oral implantology, this thus refers to bone grown right up to the implant surface without interposed soft tissue layer. No scar tissue, cartilage or ligament fibers are present between the bone and implant surface [28]. The direct contact of bone and implant surface can only be verified microscopically. An increased rate of osseointegration implants is influenced by various factors such as the tissue adequacy of implant material, design formation, surface conditions, surgical region condition, surgical tools and techniques, and finally implant loading methods. The surface condition is known to be the most crucial factor affecting osseointegration [29].

2.6 Review of Past Work

Van Thyne et al. (1954) and **Higgins et al. (2006)** reported that the low tensile strength of hcp titanium (400 MPa) can be increased to 1400 MPa by increasing the impurity levels or by the addition of alloying elements. Alloying is most commonly used to strengthen metals, but due to the complex nature of metals, only specific elements are appropriate for alloying [4, 19].

ASM Handbook (1991) and **Hari et al. (1994)** reported that the addition of zirconium to titanium increases the β -transus temperature slightly. Also, Zr is fully soluble in Ti [20, 30].

Halley et al. (1994) reported that with Zr addition, the oxidation behaviour in air becomes dramatically worse, and leads to rapid formation of ZrO_2 at temperatures above 600°C [31].

Polmear et al. (2017) reported that the alloying of titanium with zirconium leads to better solid solution hardening, thereby increasing the tensile strength by 35 – 70 MPa for each weight percent of zirconium added [9].

Donachie and Matthew (2000) found out the rough value for the strength increase per wt % of zirconium as 3.5 MPa [32].

2.7 Identified Research Gap

Based on the review of the past work done, the following research gaps were identified:

- The effect of alloying Zr addition on high temperature strength of Ti alloys have not yet been studied extensively.
- Although research has been done on the effect of the alloying elements used here, no work has been reported on all these alloying elements combined.
- The effect of wear on high temperature Ti alloys have not been studied yet.

2.8 Objectives of the Thesis

- To study the microstructural effects of Zr addition on Ti-6Al-xZr-2Sn-0.5Mo-0.5Nb-0.5Si (x = 2, 4, 6, 8) alloys.
- To study the effect of Zr on the tensile strength of based high temperature Ti alloys.
- To study the effect of Zr on the hardness of Ti alloys.
- To determine the wear rate of Ti alloys and to analyse the roughness of the wear surfaces.
- To determine the β -transus temperature of Ti-6Al-xZr-2Sn-0.5Mo-0.5Nb-0.5Si (x = 2, 4, 6, 8) alloys.
- To identify the phases present in the prepared Ti alloys.

Chapter 3 EXPERIMENTAL TECHNIQUES

3.1 Alloy Development

The test alloys were prepared by melting of pure elements by Vacuum Arc Re-melting process under the protection of an argon atmosphere. Arc melting is used for melting metals, typically to form alloys. Vacuum arc re-melting process is the principle method for production of titanium alloy ingots. Here, heating is via an electric arc struck between a tungsten electrode and metals placed in a depression (crucible) in the copper hearth. In vacuum arc melting the chamber is evacuated and then back filled with argon gas. Hence, melting is performed in argon atmosphere. A standard Tungsten Inert Gas (TIG) welding unit is used as a power source.

The basic principle of vacuum arc melting is that the heat generated by the electric arc struck between the electrode and the metals serves to melt the metals placed in the crucible to form an alloy. The molten metal then solidifies in water cooled copper crucibles. Repeated melting is performed to improve the homogeneity of the alloy. Evacuation of the chamber avoids oxidation of the melt (argon being an inert gas does not react with molten metal). The metals can be heated to a temperature in excess of 2000°C.

There are three main parts to the system: power source (TIG– 600Amp), chiller and vacuum unit [33]. The vacuum unit with rotary and diffusion pumps can attain a vacuum of 10^{-6} m bar. The cold circulation water from the chiller cools both the copper hearth and the electrodes. After elemental metals (or master alloy) are melted and solidified, it can be turned over by a tweezer mechanism without breaking the vacuum (and then re-melted). The melting → solidification → turn over of sample → re-melting process is typically repeated three times to attain a better compositional homogeneity. A typical vacuum arc melting furnace and a schematic of the furnace is shown in Figure 3.1. The main advantage of alloys obtained via vacuum arc re-melted process is the elimination of porosity in the centre, minimised macro segregation, and the

removal of dissolved gases such as hydrogen and nitrogen, giving a minimal amount of unwanted trace elements having high vapour pressures.

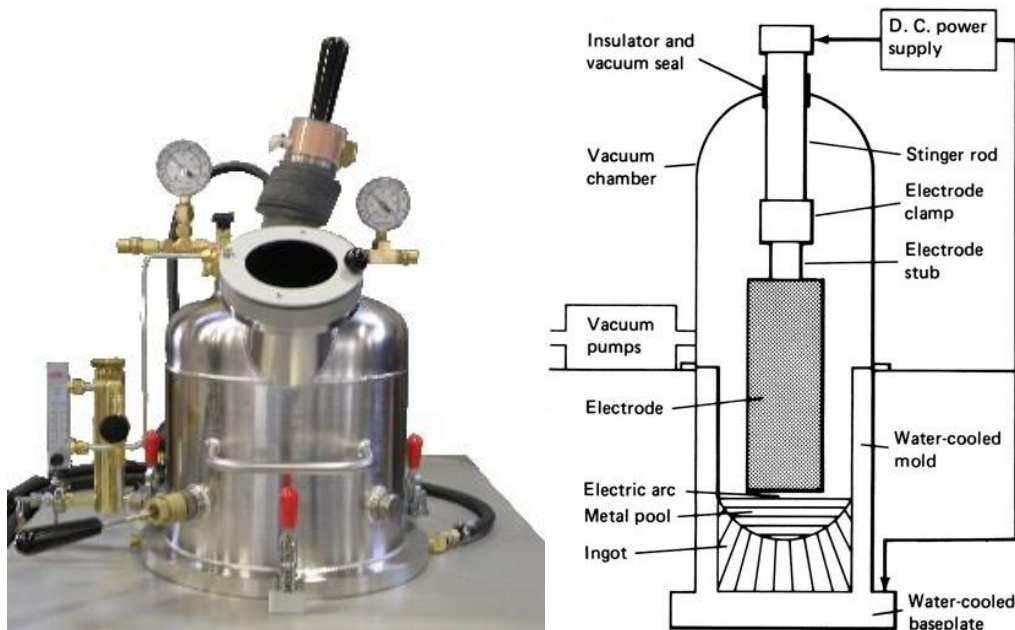


Figure 3.1: (a) Vacuum arc melting furnace (b) schematic of vacuum arc melting furnace

Titanium, aluminium, zirconium, tin, molybdenum, niobium and silicon in powdered form were weighed and fed into the vacuum arc reactor. The amount of each element taken to obtain different compositions of the alloy are mentioned in Table 3.1. Different amounts of each element were weighed to obtain four ingots (sample alloys) such that the total weight of each sample was 500g. The samples were labelled as: sample 1, sample 2, sample 3 and sample 4. The amount of the elements weighed were such that sample 1 to sample 4 were made according to increase in zirconium content, with sample 1 containing the least amount of zirconium and sample 4 containing the highest amount of zirconium. Each sample was turned and re-melted six times to achieve a better homogeneity [34]. After the solid ingot was formed, primary fabrication was carried out, during which the ingot structure was broken down by hot working and heat treatment following it [7].

Table 3.1: Raw material composition

Alloy	Weight of pure element (g)						
	Al	Zr	Sn	Mo	Nb	Si	Ti
Sample 1	30	10	10	2.5	2.5	1.5	Bal.
Sample 2	30	20	10	2.5	2.5	1.5	Bal.
Sample 3	30	30	10	2.5	2.5	1.5	Bal.
Sample 4	30	40	10	2.5	2.5	1.5	Bal.

All the ingots were hot forged at 995 °C. The samples were kept inside forging slugs coated by liquid glaze to prevent the sample from contamination by oxygen, nitrogen, hydrogen and carbon. They were then rolled in a hot rolling mill at 900 °C.

These samples were then heat treated to enhance the properties of the material. Heat treatment of materials is a fundamental metallurgical process. Titanium and titanium alloys are heat treated to achieve different properties, for example, to optimize special properties such as fracture toughness, fatigue strength, to increase strength, to produce an optimum combination of ductility, machinability and structural stability [35]. The heat treatment can be divided into two kinds: surface and bulk heat treatment. Different technologies for surface treatment aiming at improving the tribological properties of titanium alloys are being attempted. Some of the recent works include plasma-assisted surface treatments, laser-assisted surface treatments, and ion implantation. The main aim of some of these treatments is to change the microstructure of the surface layers of the materials (without changing the chemistry) via extraordinary high heating and cooling rates or the effect of the melting of the surface by laser techniques. Various types of bulk heat treatments, such as single, duplex, beta and recrystallization annealing, solution treating and aging treatments, are used to achieve selected mechanical properties [30].

Figure 3.2 shows the outline of the heat treatment process. The material was first heated to a temperature of 1100 °C at the rate of 5 °C/s. It was

maintained at that temperature with a soaking time of 2hrs, before allowing to cool by air cooling.

The material was then heated to 700 °C at the same rate of 5 °C/s, and that temperature was maintained for 4hrs. Then, the material was quenched by quickly transferring to a salt bath, containing 50 wt % NaNO_3 and 50 wt % KNO_3 to get the test alloys. Quenching is the most commonly used to harden the material and obtain desirable properties. The quenching rate must always be taken account. A very slow rate of quenching would reduce residual stresses and distortion, but may cause detrimental effects such as precipitation and increased tendency towards corrosion [36]. Then the samples were cut into the required geometry by wire EDM cutting.

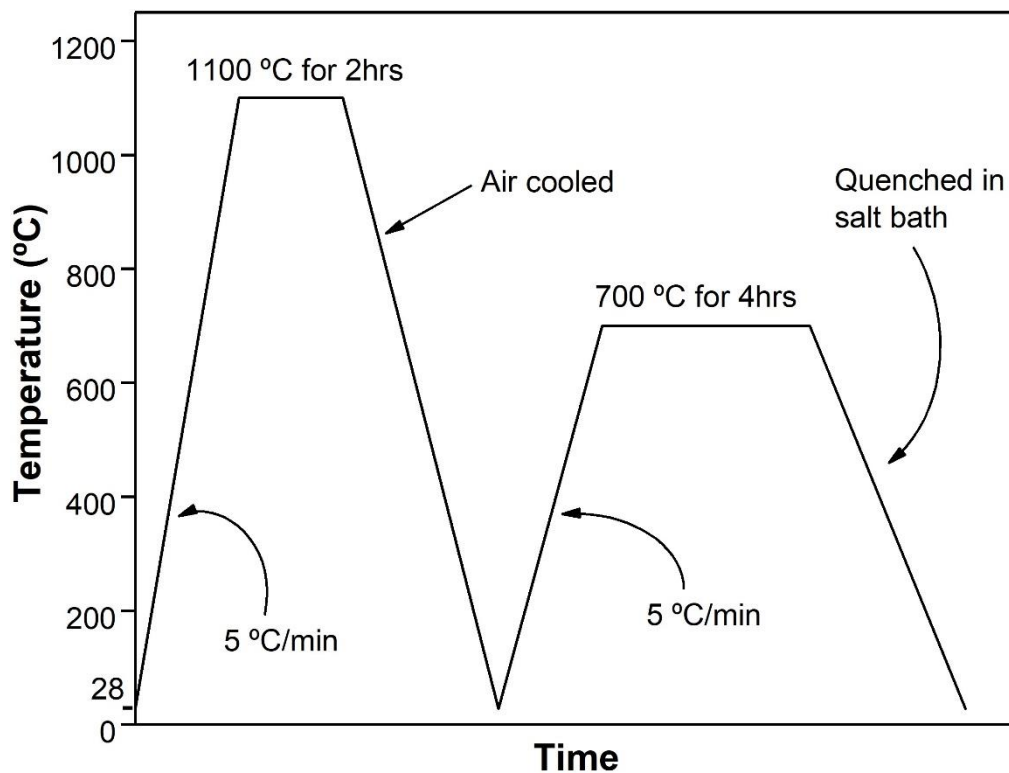


Figure 3.2: Heat treatment graph

3.2 Characterization

After the alloys were developed, their compositions were analysed, and the alloys were suitably labelled. Then, they were put forward for various tests to determine their different properties, and to check whether the alloy was developed was suitable for the present study.

Spectrophotometry is the quantitative measure of the reflection or transmission properties of a material as a function of wavelength. It deals with wavelength ranges such as near ultraviolet, near infrared and visible light. A device called spectrophotometer is used to measure the absorbance or transmittance of radiation through a sample. The spectrophotometer takes measurement at a specific wavelength, and it is possible to choose any wavelength in the spectrophotometer's register.

After the ingots were formed, each sample was put for observation in EDX 600 Spectrometer. The controller connected to the spectrophotometer controls the sample holder, and takes measurements automatically.

3.2.1 Microstructure Analysis

An optical microscope uses visible light to produce a magnified image of the specimen, which is projected onto an imaging device. The use of optical microscopy is a very effective way to analyse microstructural characteristics of a material. While the analysis tool itself is more of a subjective tool, certain quantitative analysis procedures can be used such as image processing to extract data such as average grain size and average geometric alignment.

Each sample was casted in thermosetting resins to produce non-porous uniform mounts. Buehler's SimpliMet 3000 was used for hot mounting the samples. The reason for mounting the sample is because the samples are very thin and difficult to hold while polishing, and the mount itself is very hard,

which helps reduce rounding of edges from polishing. After mounting, all the samples were polished manually on Buehler’s MetaServ 250 Grinder Polisher according to the sequence shown in Table 3.2. Velvet cloth was used for polishing with diamond paste of 0.25 micron to get a mirror finish [37]. After polishing using diamond paste, the samples were washed with ethanol. Ethanol is preferred over water because it evaporates more rapidly in comparison with water. Figure 3.3 shows the mounted samples before and after polishing.

Table 3.2 : Polishing Steps for Optical Microscopy

Paper Grade	Polishing Time (mins)	Cooling Liquid
150	20	Water
220	20	Water
320	20	Water
600	20	Water
800	20	Water
1200	20	Water
1500	20	Water
2000	20	Water
2500	20	Water
Velvet Cloth	20	Diamond Spray



Figure 3.3 : Mounted samples for microstructure analysis: (a) before polishing (b) after polishing

In order to achieve a better understanding about the particle size, the polished samples have to be chemically etched. So, a suitable etchant (Kroll's Reagent) [38] was prepared according to the composition mentioned in Table 3.3: Etchant Composition. Each specimen was swabbed with the etchant using a cotton swab for 15 seconds. The samples were rinsed again with ethanol, and dried using a hot hair dryer. Now, the samples were put under Carl Zeiss Inverted Optical Microscope Model: Axiovert.A1 for microstructure evaluation.

Table 3.3: Etchant Composition

Chemical	Volume (mL)
Distilled water	92
Hydrofluoric acid (48%)	2
Nitric acid (70%)	6

3.2.2 Tensile Test

The tensile test is one of the most commonly used tests for evaluating materials. In its simplest form, the tensile test is accomplished by gripping the opposite ends of a test specimen within the load frame of a test machine. A tensile force is then applied by the machine, which results in the gradual elongation and eventual fracture of the test specimen. The tensile test provides force extension data that can quantify several important mechanical properties of a material.

The tensile test was performed on all the samples on UTM model Tinius Olsen H50KL with constant strain rate of 0.40 mm/min. The load v/s displacement and stress v/s strain curve were obtained the software in the computer linked to the testing machine. Tensile test for Sample 1 and Sample 4 were conducted at high temperature (500 °C) as well as per ASTM D3039-76 test standards on a computerized UTM model ASI AMT-2SC. The tension test is generally performed on flat specimens. The specimen used here is shown in Figure 3.4. The ASTM standard test recommends that the length of the test specimen should be at least 250mm long. But the ingots prepared were only 40mm long. So, jigs (Figure 3.5) were made to hold the sample in place. A uniaxial load was applied through the ends. The gauge length of the specimen was 16 mm. The tests were performed with constant strain rate of 0.40 mm/min.

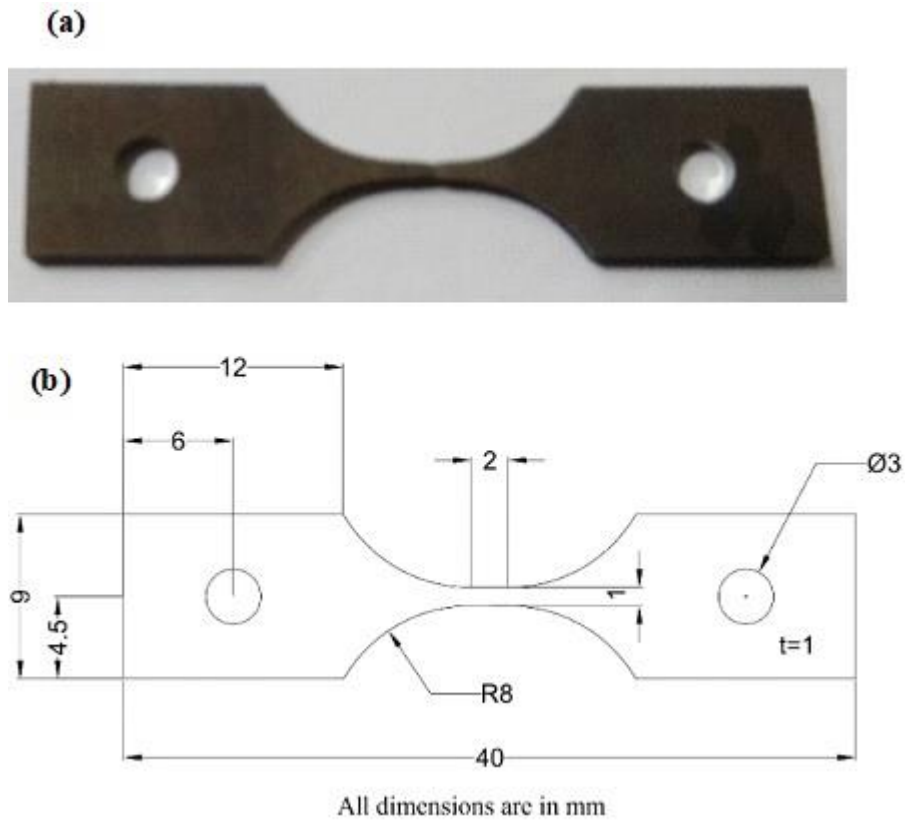


Figure 3.4: Sample for Tensile test: (a) Original sample (b) Sample dimensions in AutoCad



Figure 3.5: Jigs for tensile testing

3.2.3 Hardness Test

The term hardness is defined as the ability of the material to resist permanent deformation when in contact with an indenter under load. Generally, a hardness test consists of pressing an indenter of known geometry and mechanical properties in the test material. The hardness of the material is quantified using one of a variety of scales that directly or indirectly indicate the contact pressure involved in deforming test surface. Since the indenter is pressed into the material during testing, hardness is also viewed as the ability of the material to resist compressive loads. The indenter maybe spherical (Brinell test), pyramidal (Vicker's and Knoop test), or conical (Rockwell test). In the Brinell, Vicker's and Knoop tests, hardness value is the load supported by unit area of indentation, expressed in kilograms per square millimetre (kgf/mm²). Here, Rockwell hardness test was used to find the macro-hardness of the material.

Rockwell hardness test determines the hardness of a material using the indentation penetration depth of the indenter, and compares it to that of a reference material. The correct notation for Rockwell hardness value is HR followed by the scale, for example 56 HRC, where C is the letter for the scale used.

The Rockwell hardness test is administered by applying the predetermined minor force to the sample, increasing it to the predetermined final test force, and returning to the minor test force. The difference of the two penetration depth measurements (h) is in mm. Using h , the Rockwell hardness is calculated from the following equation:

$$HR = 100 - \frac{h}{0.002}$$

Once the tensile test was carried out, one broken part from each of the samples was used for hardness measurement by Rockwell Hardness test using Digital Rockwell Hardness Tester AMT-5 by ASI. A 120° diamond

spheroconical indenter was used with a 150 kgf force with a dwell time of 10 seconds. Each sample was tested at least three times at different positions, and their average was taken as the hardness value of that sample. The sample after hardness test is shown in Figure 3.6: Sample after Rockwell hardness test.



Figure 3.6: Sample after Rockwell hardness test

3.2.4 Wear Test

Fretting is a phenomenon that occurs at the interface between two surfaces in contact in the presence of cyclic load, which gives rise to a small relative displacement [39, 40]. Fretting usually happens where the contact surfaces are not supposed to move relatively to each other [41]. Fretting wear is the removal of material between two surfaces in contact, with oscillated micro relative slip under contact pressure. The nature of fretting involves a large number of factors including both mechanical properties and the working environment, such as the applied normal load, roughness of the contact surfaces, and material properties. It is observed mainly in mechanical assemblies such as keyway-shaft couplings, shrink-fitted couplings, dovetail blade disc assemblies, hip joint implants, etc. When two surfaces are in contact and sliding over each other, the accumulation of particle detachment (wear) can be observed on either one or both the surfaces. Wear is divided mainly into six categories: adhesion, abrasive, fatigue, corrosion, erosion and electrical arc [42]. Many parameters affect fretting behaviour. The primary variables that directly affect fretting behaviour are normal load, coefficient of friction and slip amplitude [43]. The classical equation for sliding wear [44] is based on the theory of asperity

contact, and has been validated against pin-on-ring sliding tests for a series of materials [45]. It is known as the Archard equation, which can be written as:

$$\boxed{\frac{V}{s} = K \frac{P}{H}}$$

V = wear volume;

s = sliding distance;

K = dimensionless wear coefficient;

P = normal load; and

H = hardness of the material

The Archard wear equation links the loss of material volume to the product of the sliding distance by the normal load. It describes the severity of wear by means of the wear coefficient. For engineering applications, the quantity K/H is more useful. This is called the dimensionless wear coefficient (k).

Fretting is a phenomenon that occurs at the interface between two surfaces in contact in the presence of cyclic load, which gives rise to a small relative displacement [39, 40]. Fretting usually happens where the contact surfaces are not supposed to move relatively to each other [41]. Fretting wear is the removal of material between two surfaces in contact, with oscillated micro relative slip under contact pressure. The nature of fretting involves a large number of factors including both mechanical properties and the working environment, such as the applied normal load, roughness of the contact surfaces, and material properties. It is observed mainly in mechanical assemblies such as keyway-shaft couplings, shrink-fitted couplings, dovetail blade disc assemblies, hip joint implants, etc. When two surfaces are in contact and sliding over each other, the accumulation of particle detachment (wear) can be observed on either one or both the surfaces. Wear is divided mainly into six categories: adhesion, abrasive, fatigue, corrosion, erosion and electrical arc [42]. Many parameters affect fretting behaviour. The primary variables that directly affect fretting

behaviour are normal load, coefficient of friction and slip amplitude [43]. The classical equation for sliding wear [44] is based on the theory of asperity contact, and has been validated against pin-on-ring sliding tests for a series of materials [45]. It is known as the Archard equation, which can be written as:

$$\boxed{\frac{V}{s} = K \frac{P}{H}}$$

V = wear volume;

s = sliding distance;

K = dimensionless wear coefficient;

P = normal load; and

H = hardness of the material

The Archard wear equation links the loss of material volume to the product of the sliding distance by the normal load. It describes the severity of wear by means of the wear coefficient. For engineering applications, the quantity K/H is more useful. This is called the dimensionless wear coefficient (k).

A purpose built fretting wear test machine was used to investigate the fretting wear quantitatively with appropriate material combinations on a reciprocating wear test machine. The normal load between the fixed and moving heads was applied via a dead weight loading method. A data acquisition and evaluation strategy was developed for the characterisation of the mechanical contact response. It was based on the contact displacement and normal load.

Different combinations of normal load applied and were employed to evaluate the fretting wear characteristic of the materials. Normal loads of 10 N, 20 N and 30 N were applied for 20 min each at cyclic frequencies of 8.5 Hz and 17 Hz. The loss in mass was measured after each test, and this change in mass was used to calculate the volume loss and wear rate.

The techniques most generally applied to study changes in surface topography of wear samples are microscopy, interferometry and profilometry. Microscopy is essentially qualitative, and interferometry can only be applied to very smooth surfaces. Carl Zeiss Inverted Optical Microscope Model: Axiovert.A1 was employed to investigate the surface topography of the wear surface. It allows the specimen to be investigated without subjecting it to strain or further wear.

3.2.5 Roughness Test

Surface roughness often shortened to roughness, is a component of surface texture. It is quantified by the deviations in the direction of the normal vector of a real surface from its ideal form. If these deviations are large, the surface is rough; if they are small, the surface is smooth. Roughness is typically considered to be the high-frequency, short-wavelength component of a measured surface. However, in practice it is often necessary to know both the amplitude and frequency to ensure that a surface is fit for a purpose. Some of the parameters used to define roughness are R_a , R_q , R_z , R_{max} and R_t .

Average surface roughness (R_a) is the arithmetic average of the absolute values of roughness profile ordinates as shown in Figure 3.7. Maximum surface roughness (R_{max}) is the height between the deepest valley and the highest peak on the evaluation length. Root mean square surface roughness (R_q) corresponds to the standard deviation of the height distribution, defined on the sampling length. R_t is the maximum height of the profile. Single roughness depth (R_{zi}) is the vertical distance between highest peak and the deepest valley of the profile within a sampling length. Depth of surface roughness (R_z) is the arithmetic mean of consecutive sampling lengths. Maximum profile peak height (R_p) is height of the highest peak from the mean line, defined on the sampling length. Maximum profile valley depth (R_v) is depth of the deepest valley from the mean line, defined on the sampling length.

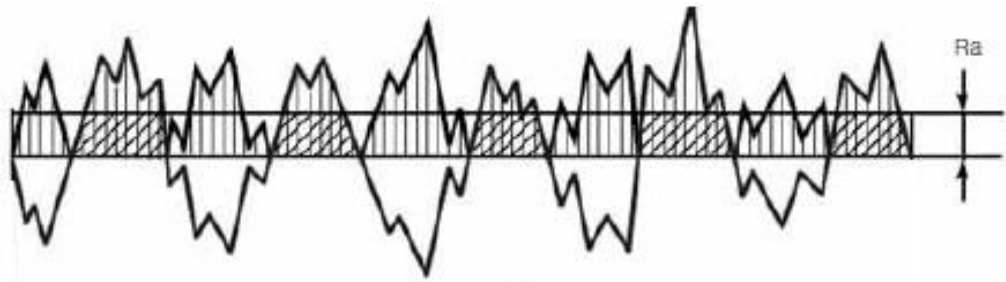


Figure 3.7: Typical surface roughness profile

The wear surfaces were checked for roughness before and after the wear test was conducted. Five parameters of surface roughness, namely average surface roughness (R_a), root mean square roughness (R_q), depth of surface roughness (R_z), maximum surface roughness (R_{max}) and maximum height of the profile (R_t) were measured using 3D surface roughness cum contour tracer on Mahr Surf from Mahr Metrology, Germany model LD-130 (Figure 3.8).



Figure 3.8: Roughness Test Instrument

3.2.6 Differential Scanning Calorimetry (DSC)

DSC testing is one of the many test methods used to measure transformation temperatures of alloys. It is a thermal method that measures the change in heat flow, which is associated with the martensitic and austenitic phase transformations through a controlled cooling/heating cycle. In the DSC procedure, the differential heat flow required to heat or cool the experimental and reference samples at the same scanning rate is recorded as a function of temperature to yield the spectrum or thermogram. The start and finish temperatures of each phase transformation can be determined from tangent lines, where the DSC curve deviates from the adjacent baselines.

10 mg of each sample was carefully cut weighed and used for DSC characterization. The experiments were conducted using an empty reference crucible following ASTM F2004 standard on Netzch DSC 214 Polyma DSC apparatus. During the test, the samples underwent a temperature change from 100 °C to 600 °C with a heating rate of 20 °C/min. In order to avoid oxidation of the alloy at high temperature, measurements were performed under flowing argon.

3.2.7 X-Ray Diffraction (XRD)

X-ray diffraction is a powerful characterization technique used in the analysis of crystalline solids that exhibit long range order, i.e. when the atomic positions are repeated in a regular fashion. When impacted by light or radiation, a 3-dimensional array of atoms, molecules or ions, cause the light to be diffracted, as described by W. H. Bragg and W. L. Bragg in 1913. This behaviour is summarized by the expression:

$$n\lambda = 2d \sin\theta$$

λ = wavelength of radiation used (1.5408Å);
d = interplanar spacing within the crystalline solid;

Θ = the incident angle between the x-rays and sets of parallel planes in the crystalline solid.

In order for diffraction to be observed (constructive interference), Bragg's law must be satisfied.

When the x-rays are scattered by the electron clouds of atoms and constructive interference occurs, the result is recorded as a distinctive powder pattern, plotted as intensity v/s 2Θ , where 2Θ is the sum of the angle of incidence and the angle of reflection. Powder patterns for pure phase or mixed powders exhibit peaks at specific values of 2Θ , yielding a characteristic fingerprint, which can be used to identify a crystalline phase or mixture of phases. The values observed for the d spacing are determined by the size and lattice centering of the crystal lattice. The intensities observed are determined by several contributing factors including the identity and positions of the atoms in the lattice, their interaction and absorption of the x-rays. The thermal motion of the scatterers as well as the geometry of the diffraction experiment can cause peak positions to shift slightly along 2Θ . During XRD experiment, an x-ray source is provided and directed at the crystalline solid sample. The sample does not need to be a single crystal, but can be a collection of crystalline solids present in a powder. The x-ray source directed at the sample diffracts based on the d-spacing and crystal lattices. These diffracted rays are measured at certain angles to view intensity. This in conjunction with the angle of incidence yields the 2Θ plot, better known as the characteristic powder pattern of the sample. The measured powder pattern and its d spacing can be searched against a database of known crystalline materials in order to identify the phase(s) present in the samples.

X-ray powder diffraction characterization was carried out using Bruker-D2 Phase diffractometer with Cu- K_{α} radiation ($\lambda=1.5418 \text{ \AA}$), and an applied voltage of 45 kV and current 40 mA. The scanning range (2Θ) was employed from 30° to 75° . The resulting peaks were fitted by X'Pert HighScore Plus software.

Chapter 4 RESULTS AND DISCUSSION

This chapter presents all the results obtained from different aspects of material testing with detailed discussion. The results of a schematic study to investigate the effects of alloying addition are provided. The results of microstructure study is presented.

The composition of the alloys were found out by Energy-dispersive X-ray spectroscopy (EDS) and are shown in Table 4.1. The alloys were labelled as samples 1, 2, 3 and 4 in increasing order of Zr content with sample 1 having 2% Zr (lowest) and sample 4 having 8% Zr (highest).

Table 4.1: Alloy composition

Alloy	Chemical composition (wt %)					
	Al	Zr	Sn	Mo	Nb	Si
Sample 1	6.02	2.06	2.01	0.504	0.501	0.34
Sample 2	5.97	4.08	1.98	0.51	0.48	0.31
Sample 3	6.016	5.98	2.04	0.488	0.506	0.34
Sample 4	6.03	8.05	2.03	0.502	0.51	0.298822

4.1 Optical Micrograph

Figure 4.1(a-d) and Figure 4.1(e-h) respectively show the optical micrographs of sample 1 to sample 4 at 50x and 100x magnifications.

The microstructure of the alloys are composed of coarse and long α lamellae structure, and no β phase. It can be observed from the micrographs that the thickness of the lath decreases as the zirconium content increases. The thickness decreased from around 5 μm in sample 1 to about 2 μm in the case of sample 4.

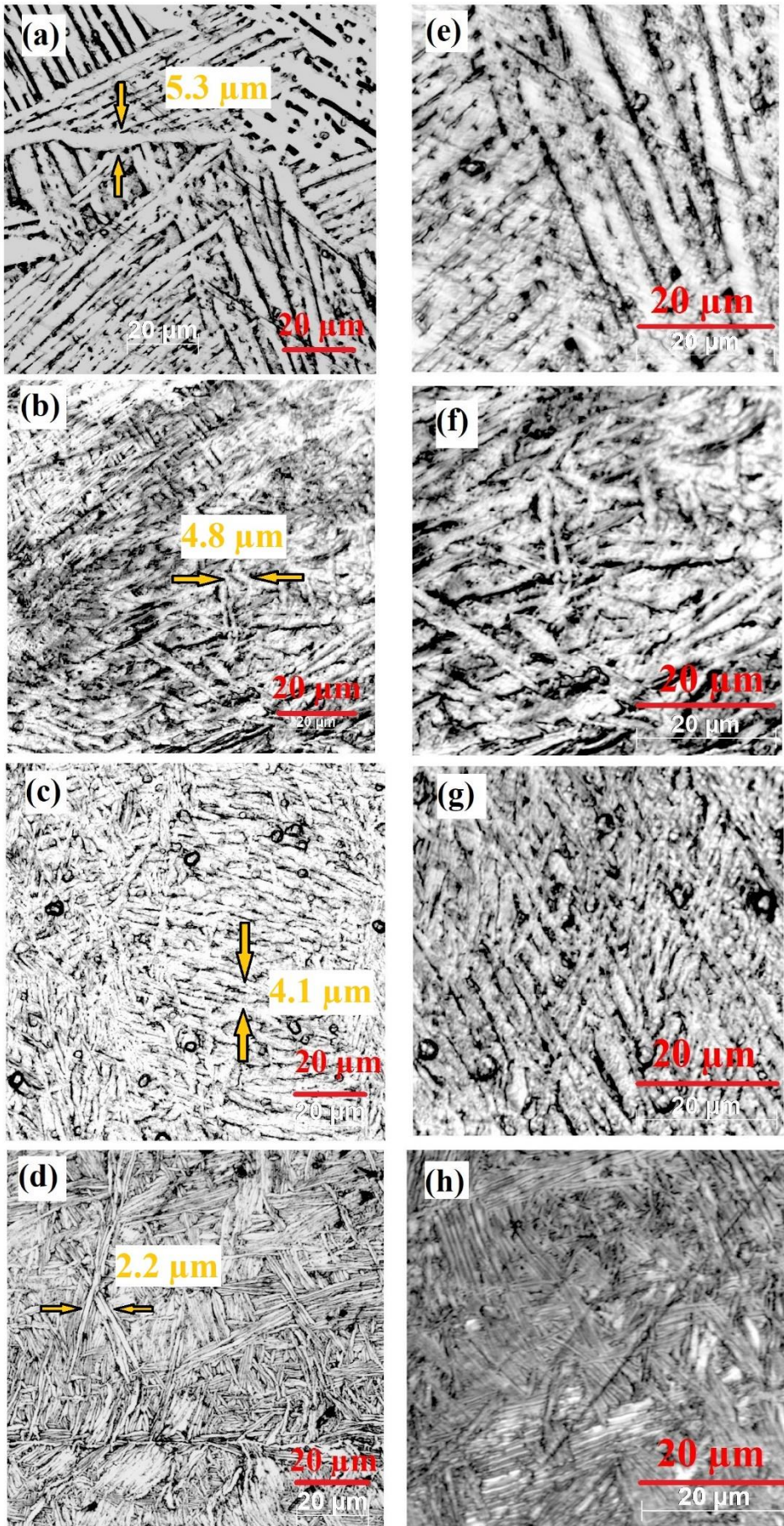


Figure 4.1: Optical micrograph at 50x (a-d) and 100x (e-h) magnifications

The lath size was found to be 5.3 μm in sample 1 (Figure 4.1-a&e), 4.8 μm in sample 2 (Figure 4.1-b&f), 4.1 μm in sample 3 (Figure 4.1-c&g) and 2.2 μm in sample 4 (Figure 4.1-d&h). It was found that the thinner the lath size, the higher was the strength of the alloy. It is because the presence of zirconium enhanced the barrier performance of the alloy, hindering the formation of β phase in the alloy, and also diffusing into areas with lower concentration of β . This is why the thinnest α structures were observed in the alloy with highest zirconium content.

Also, some dark spots were observed in the lower Zr content samples, which may correspond to the formation of silicide precipitates in the alloy. Though this was not found in the highest Zr content alloy. This has to be confirmed with scanning electron microscopy (SEM) or transmission electron microscopy (TEM) analysis.

4.2 Tensile Test

Figure 4.2 shows the tensile test specimen before and after experiment was performed. Figure 4.3 shows the stress v/s strain curves for Ti-6Al-xZr-2Sn-0.5Mo-0.5Nb-0.3Si ($x = 2, 4, 6, 8$) at room temperature. The results obtained from tensile testing at room temperature are tabulated in Table 4.2.



Figure 4.2: Tensile test specimen

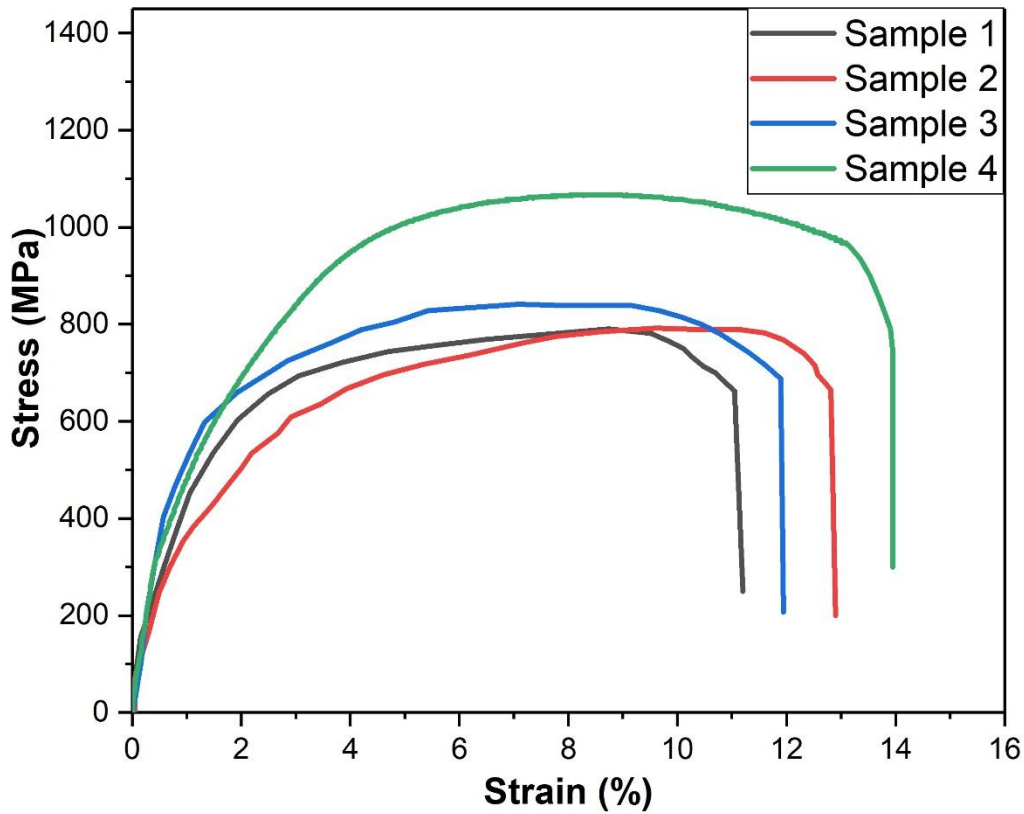


Figure 4.3: Stress - strain graph at RT

Table 4.2: Tensile test result at room temperature

Material	Yield Strength (MPa)	Ultimate Tensile Strength (MPa)	Rupture Point (MPa)	Elongation (%)
Sample 1	620 ± 10	785 ± 10	568 ± 10	12 ± 0.5
Sample 2	660 ± 10	790 ± 10	620 ± 10	12.4 ± 0.5
Sample 3	685 ± 10	823 ± 10	693 ± 10	13.1 ± 0.5
Sample 4	957 ± 10	1067 ± 10	745 ± 10	13.7 ± 0.5

It is found that the yield strength for highest Zr content alloy is 957 MPa as compared to 685 MPa, 660 MPa and 620 MPa in the lower Zr content alloys.

The tensile strength of Ti-6Al-xZr-2Sn-0.5Mo-0.5Nb-0.3Si (x = 2, 4, 6, 8) is found to increase with increasing Zr content. The tensile strength values were 1067 MPa and 785 MPa for high and low Zr content alloys respectively.

When the length of the samples after failure was checked, it was found that all the samples had similar elongation (12 %) at room temperature.

Sample 1 and sample 4 (the alloys with least and most amount of zirconium content respectively) were tested for tensile strength at 500 °C. The results are shown in Table 4.3. Analysis of the stress – strain curve obtained showed that the tensile strength and yield point decreased with the increase in temperature (as expected) as shown in Figure 4.4 and Figure 4.5. It was also noted that although the tensile properties decreased, the tensile strength of higher zirconium content alloy was much higher than that of lower zirconium content alloy even at 500 °C.

The tensile properties of samples 1 and 4 tested at high temperature of 500 °C are displayed in Table 4.3. As expected, the tensile strength and yield strength of the alloys decreased when tested at 500 °C. Even then, the difference between ultimate tensile strength and yield strength was relatively low. Due to the increase in temperature, the percentage reduction in ultimate tensile strength was 29% for sample 1 compared to 20% in sample 4. The yield strength reduction percentage was 23% for sample 1, while it was 22% for sample 4. The result indicates that the ultimate tensile strength and the yield strength of sample 4 remained quite high even at high temperature. This suggests that the Ti-6Al-8Zr-2Sn-0.5Mo-0.5Nb-0.3Si might be a good choice for aircraft frame material.

Table 4.3: Tensile properties

Sample	Yield Strength (MPa)		Ultimate Tensile Strength (MPa)	
	24 °C	500 °C	24 °C	500 °C
Sample 1	620 ± 10	490 ± 10	785 ± 10	551 ± 10
Sample 4	957 ± 10	750 ± 10	1067 ± 10	850 ± 10

The ultimate tensile strength and yield strength of the alloys at room temperature and at high temperature (for sample 1 and sample 4) are graphically represented in Figure 4.6 and Figure 4.7 respectively.

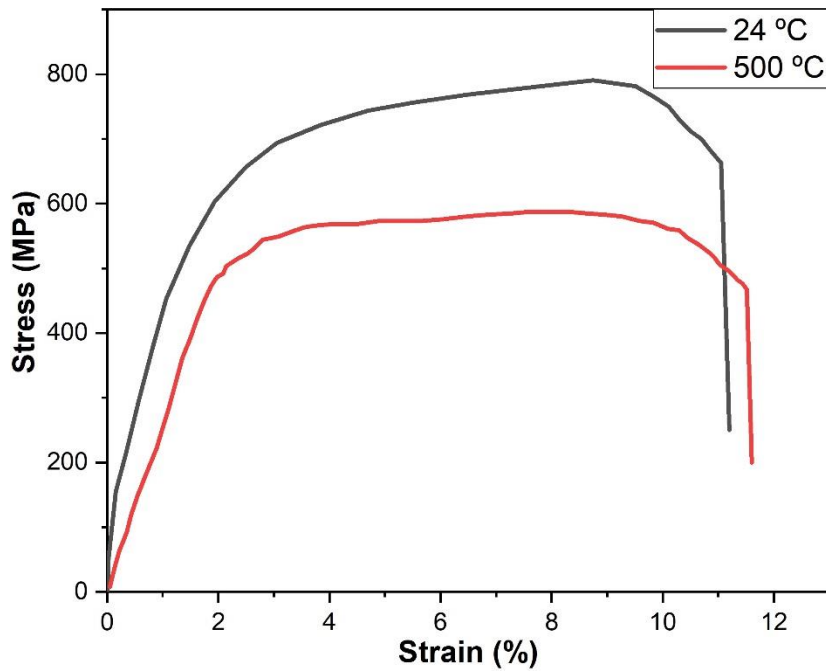


Figure 4.4: Stress-strain curve of lowest Zr content alloy

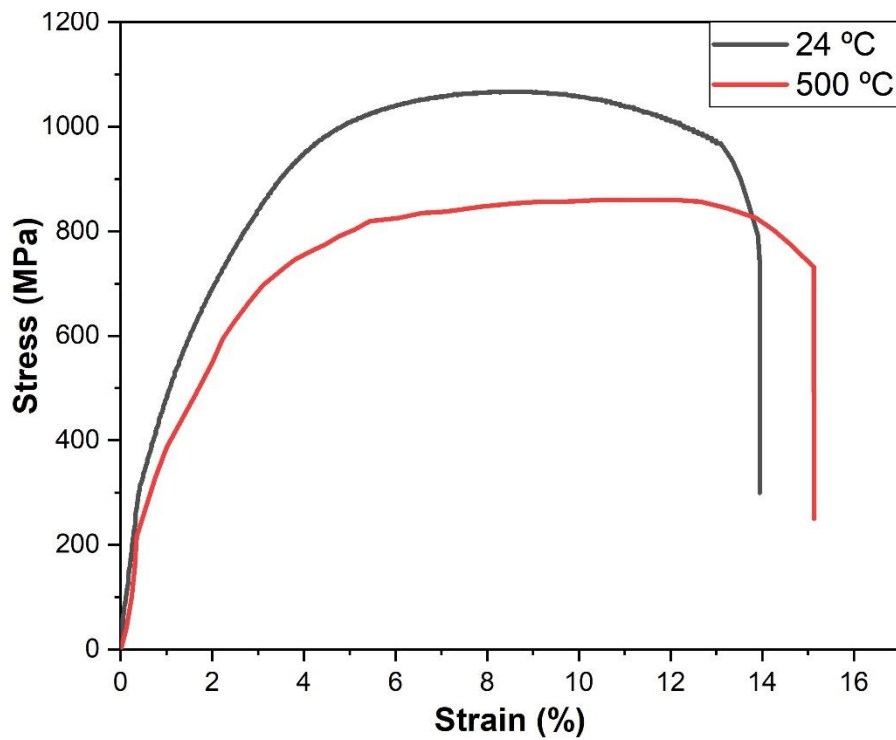


Figure 4.5: Stress-strain curve of highest Zr content alloy

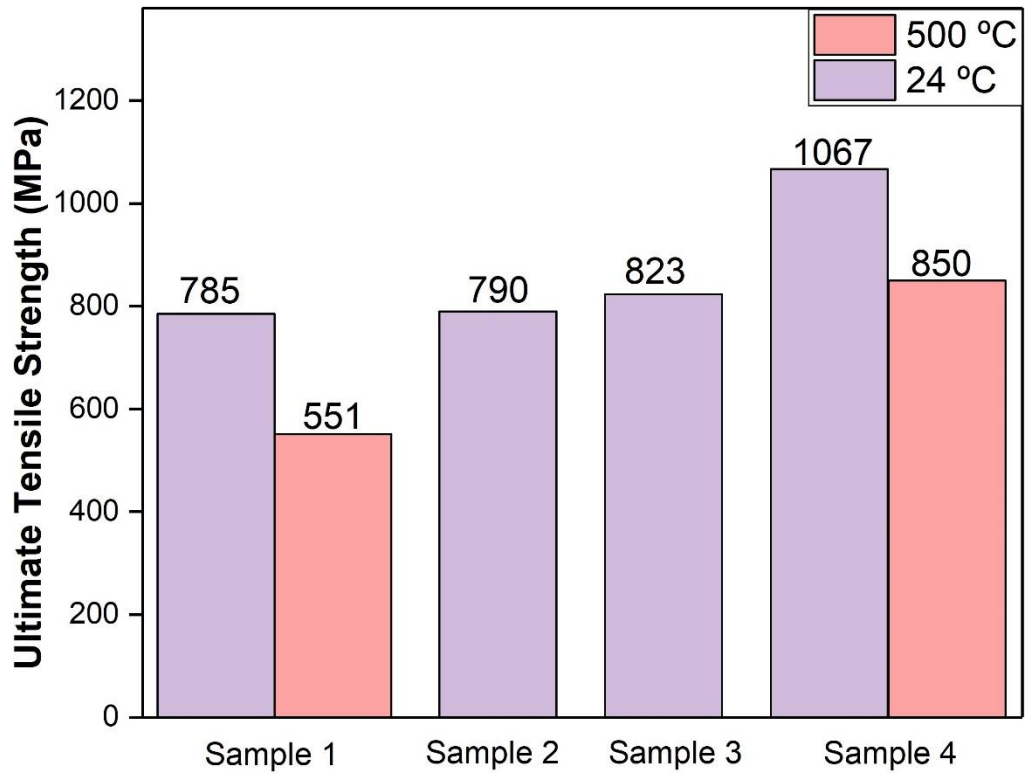


Figure 4.6: Ultimate tensile strength values

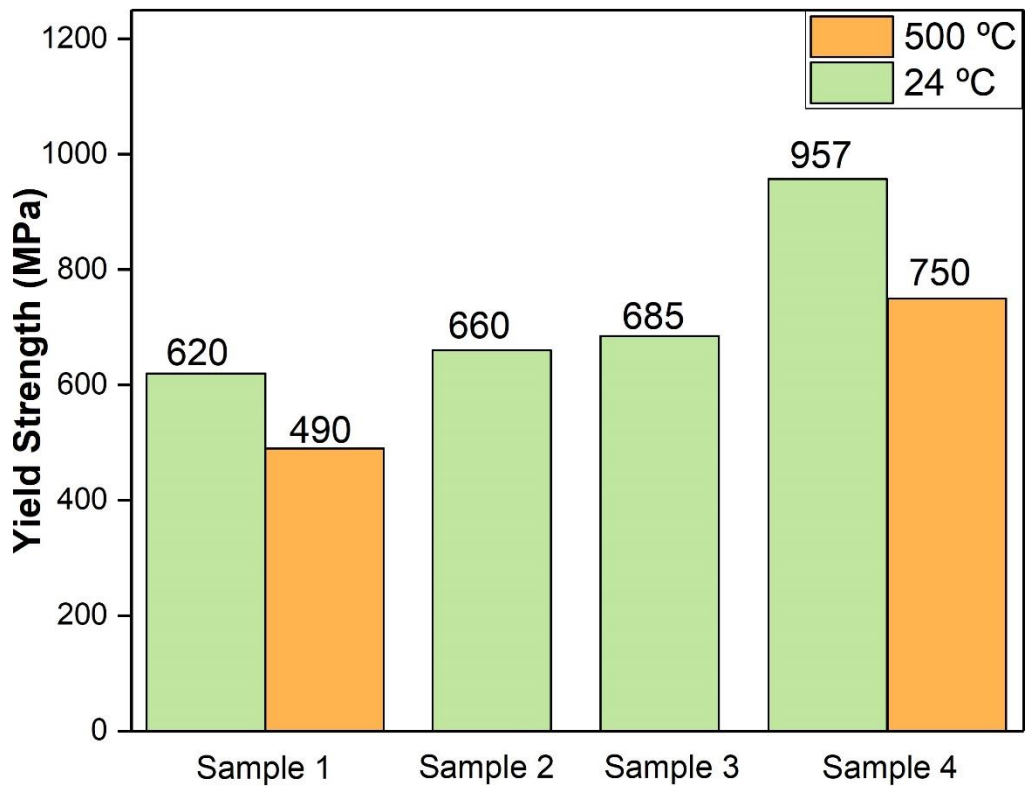


Figure 4.7: Yield strength values

4.3 Hardness Test

Figure 4.8 show the results obtained from the Rockwell hardness test. The macrohardness of the alloy samples were found to increase as the zirconium content increased. Ti-6Al-8Zr-2Sn-0.5Mo-0.5Nb-0.3Si alloy showed the highest hardness value of all the four samples prepared. The hardness of pure Ti (150 HV) is found to be very less compared to the hardness value of Ti-6Al-8Zr-2Sn-0.5Mo-0.5Nb-0.3Si alloy (329 HV) [7].

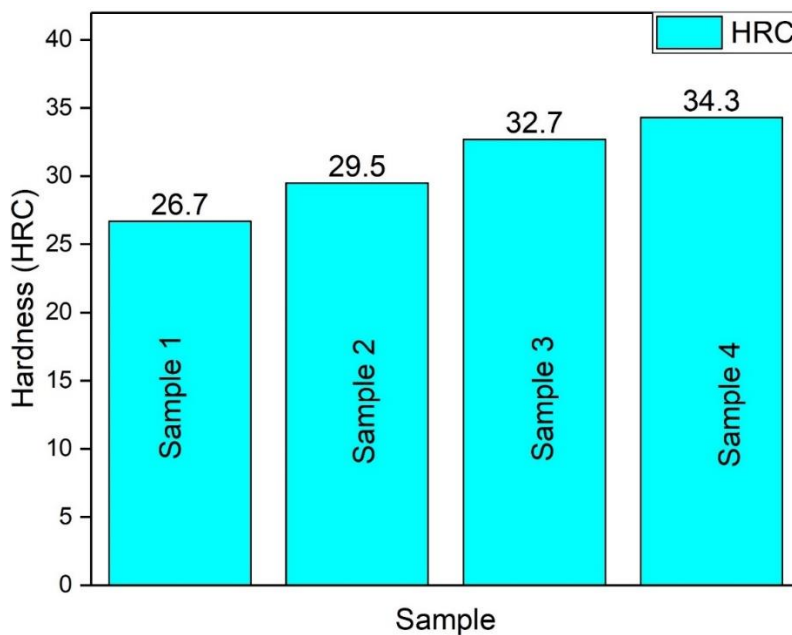


Figure 4.8: Rockwell Hardness test results at RT

The obtained hardness values obtained were compared with standard values from conversion charts [46-48]. The chart shows the tensile strength of titanium alloy at specific values of hardness. The tensile values obtained experimentally were in accordance with the tensile values for that particular hardness value. These tensile values given in the conversion charts are mentioned in Table 4.4 along with the experimental value of tensile strengths.

Table 4.4: Comparison of Tensile strength

Sample	Rockwell Hardness (HRC)	Experimental Tensile Strength (MPa)	Tensile Strength from conversion chart (MPa)
Sample 1	26.7 ± 0.2	785 ± 10	796
Sample 2	29.5 ± 0.2	790 ± 10	866
Sample 3	32.7 ± 0.2	823 ± 10	892
Sample 4	34.3 ± 0.2	1067 ± 10	1075

4.4 Wear Analysis

Figure 4.9 and Figure 4.10 respectively shows the volume loss occurred during wear test at cyclic frequencies of 8.5 Hz and 17 Hz for different loads. It was observed that the wear volume loss increased linearly with an increase in applied load in both the cases. This is due to the increase in friction force with increase in load. It was also observed that the maximum volume loss was observed in sample 1 compared to the minimum volume loss in sample 4.

The wear coefficient was calculated at 8.5 Hz and 17 Hz for loads of 10N, 20 N and 30 N. The results are respectively presented in Figure 4.11 and Figure 4.12.

Figure 4.13 and Figure 4.14 respectively represent the optical micrographs of samples 1-4 at 5x magnification before and after wear test was conducted. The roughness values of some samples are also mentioned.

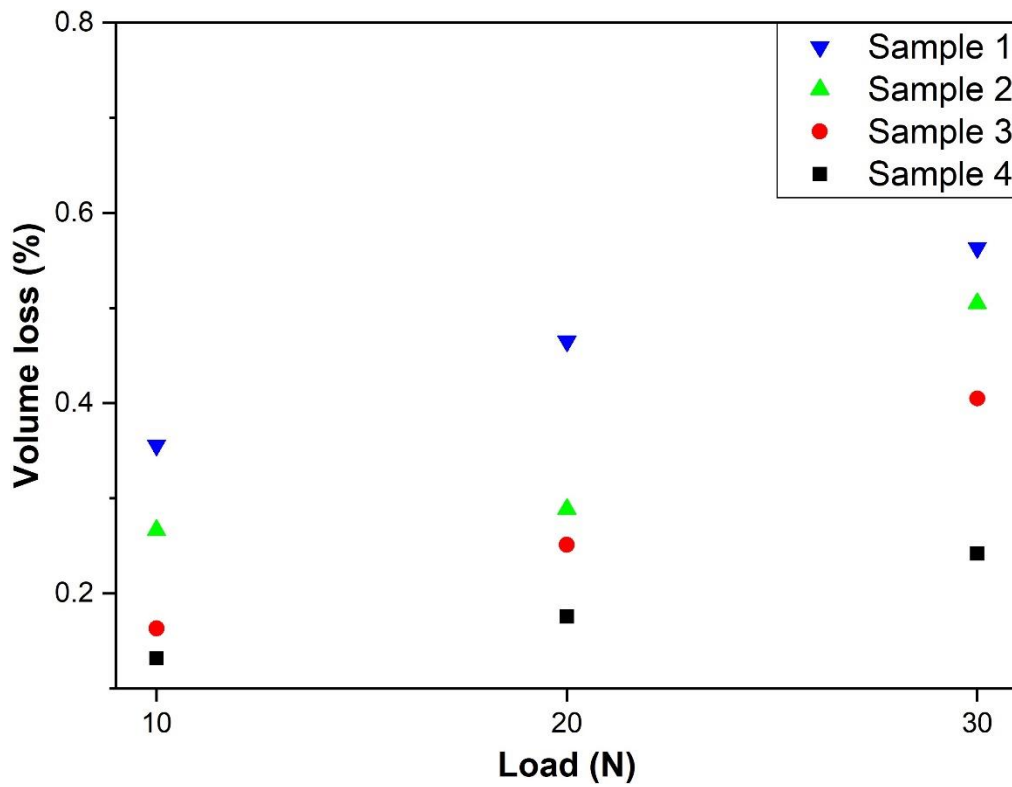


Figure 4.9: Volume loss at 8.5 Hz

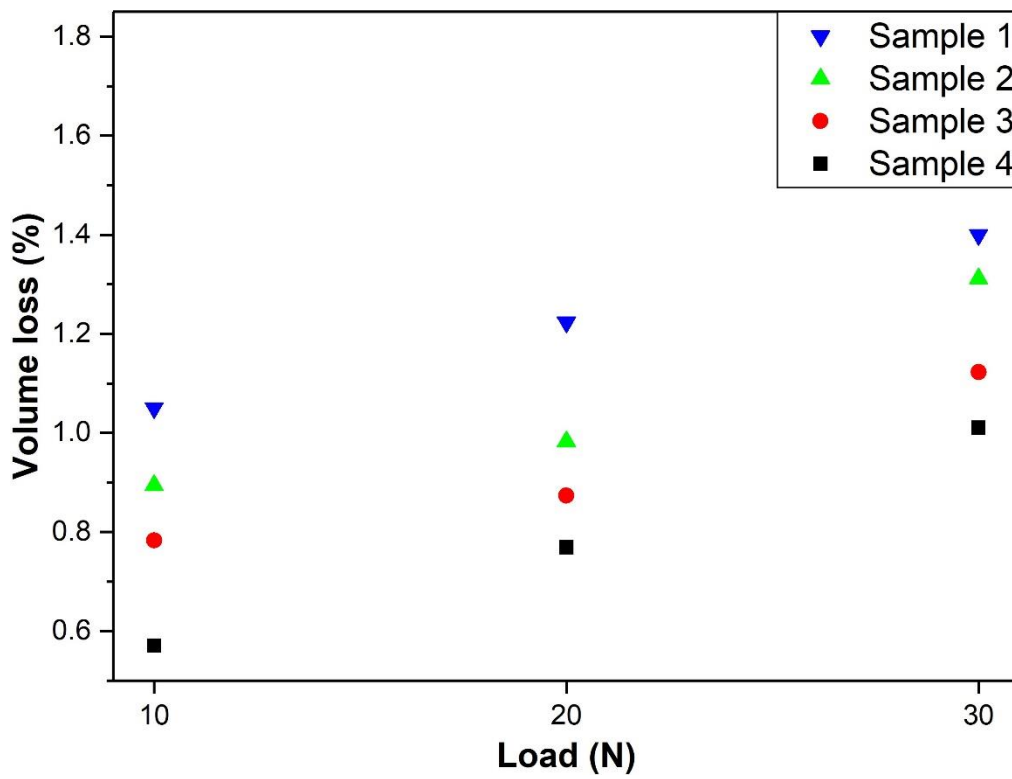


Figure 4.10: Volume loss at 17 Hz

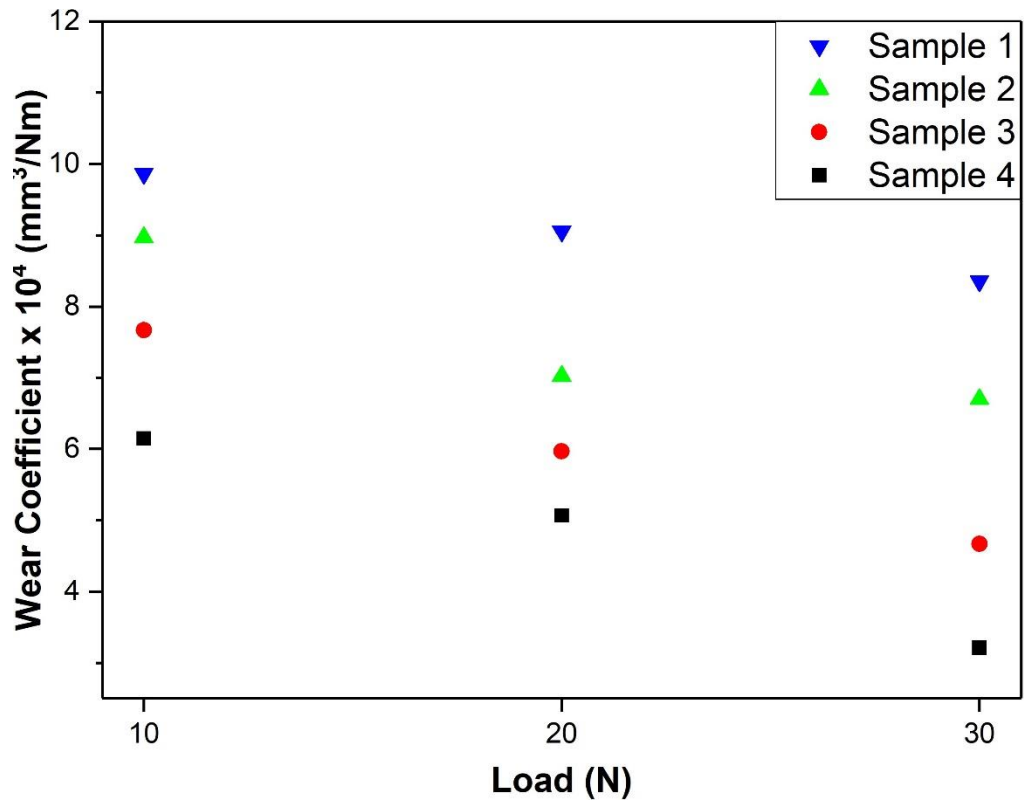


Figure 4.11: Wear coefficient v/s load at 8.5 Hz

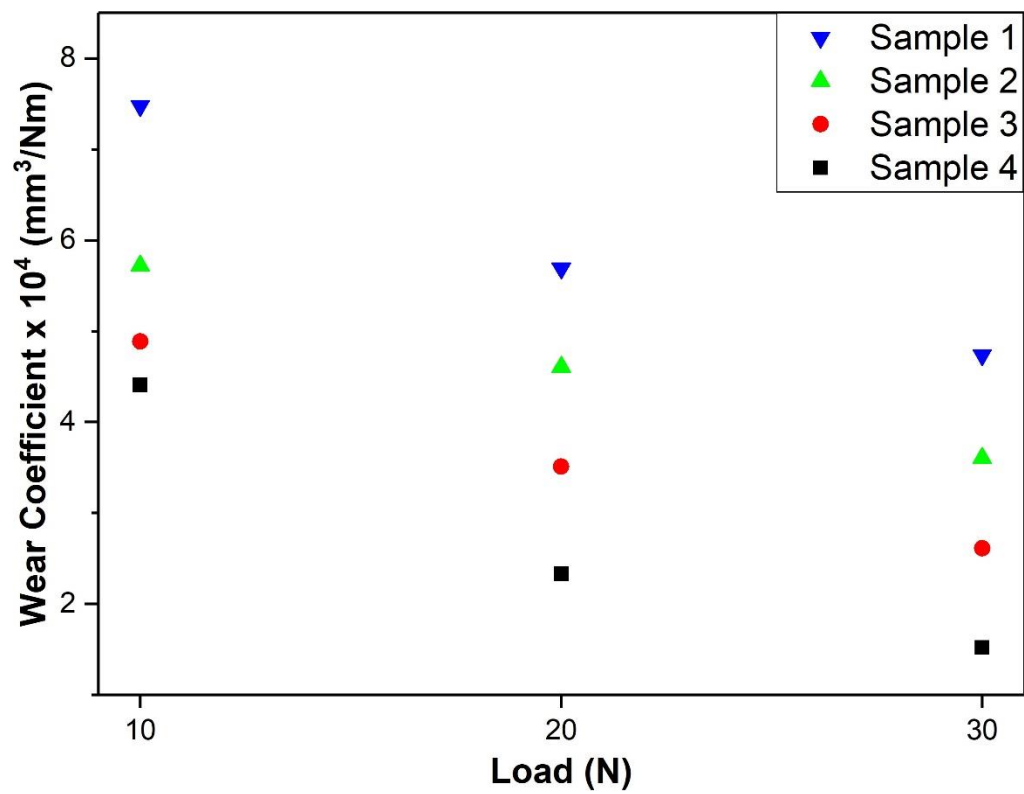


Figure 4.12: Wear coefficient v/s load at 17 Hz

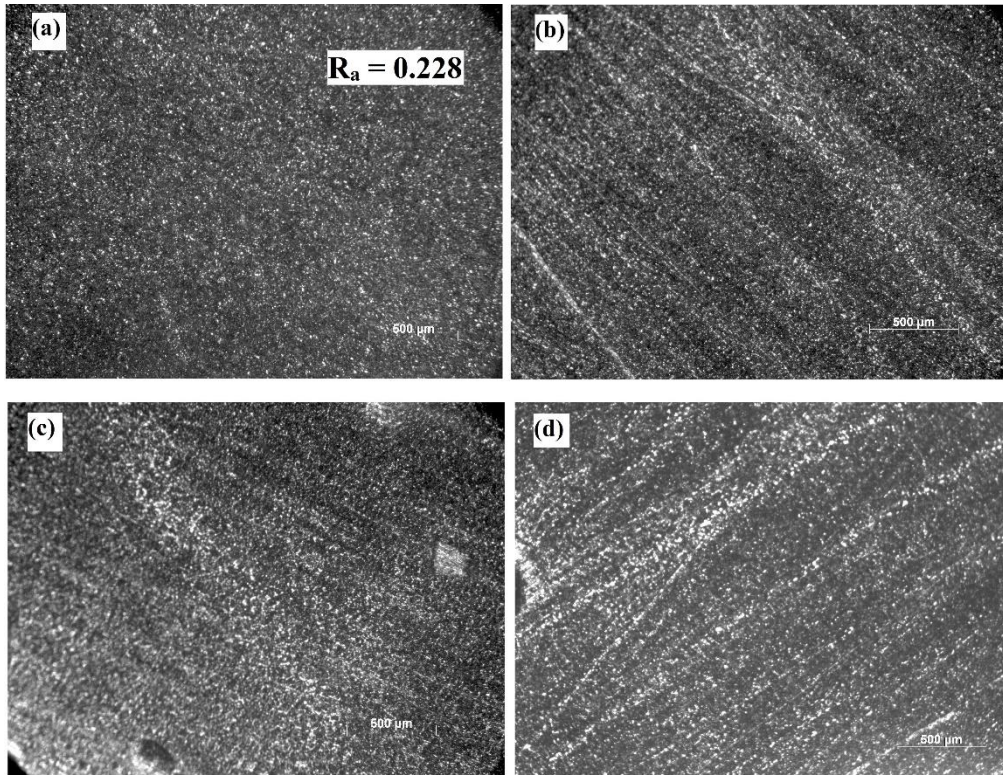


Figure 4.13: Optical micrograph before wear test of (a) Sample 1 (b) Sample 2 (c) Sample 3 (d) Sample 4

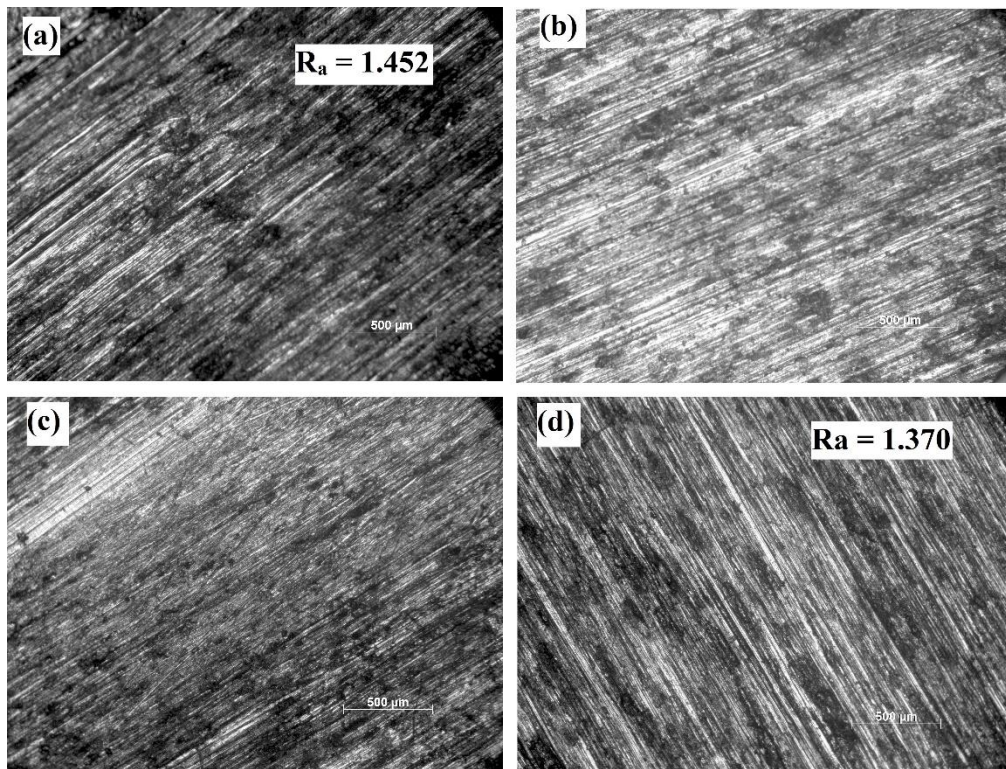


Figure 4.14: Optical micrograph after wear test of (a) Sample 1 (b) Sample 2 (c) Sample 3 (d) Sample 4

4.5 Roughness Analysis

To properly analyse the wear surface, roughness test was performed on the wear surface before and after subjecting to wear test. Figure 4.15(a) shows the roughness profile of the sample before wear test. Figure 4.15(b&c) respectively show the roughness profile of sample 4 and sample 1. The surface roughness measurements of the same are tabulated in Table 4.5.

It was observed that the roughness of the material changed drastically when subjected to wear, with the maximum surface roughness ($9.147 \mu\text{m}$) in the case of sample 1 compared to only $8.802 \mu\text{m}$ in the sample with the highest zirconium content. Although there wasn't much difference in the depth of surface roughness, it was $9.910 \mu\text{m}$ (highest) in sample compared to $9.137 \mu\text{m}$ (lowest) in sample 4.

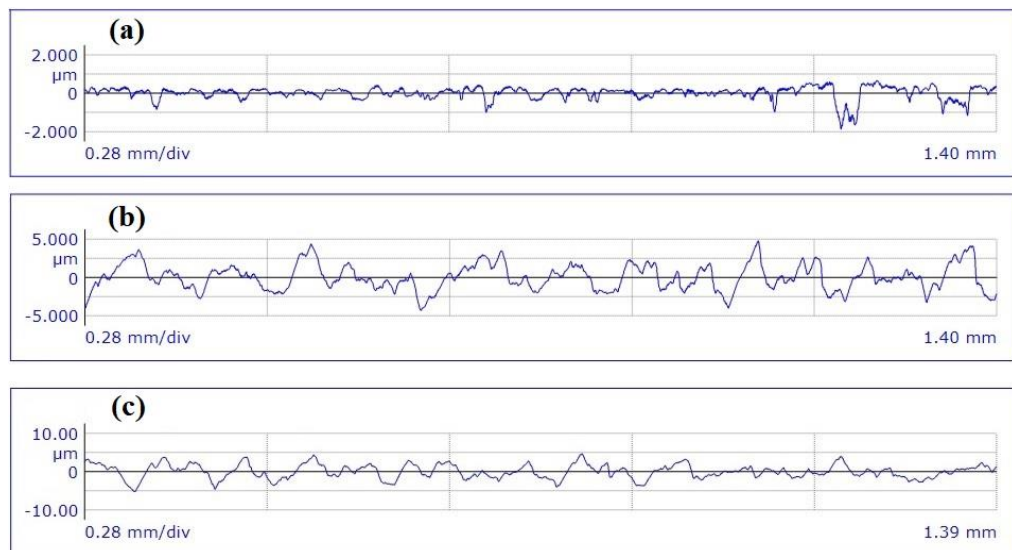


Figure 4.15: Roughness profile of (a) Sample1 before wear test (b) Sample1 (c) Sample 4 after wear test

Table 4.5: Roughness profile parameters

Sample	R_a (μm)	R_q (μm)	R_z (μm)	R_{max} (μm)	R_t (μm)
Before Wear	0.228	0.327	1.510	2.546	2.546
Sample 1	1.452	1.800	7.940	9.147	9.910
Sample 4	1.370	1.697	7.662	8.802	9.137

4.6 Differential Scanning Calorimetry (DSC)

The heat flux graph obtained from performing DSC experiment is presented in Figure 4.16. No significant peak was observed in any of the samples, meaning no phase change ($\alpha \rightarrow \beta$ transition) has happened in any of the alloys under study at least until 600 °C. So, all the four alloys can withstand high temperature applications.

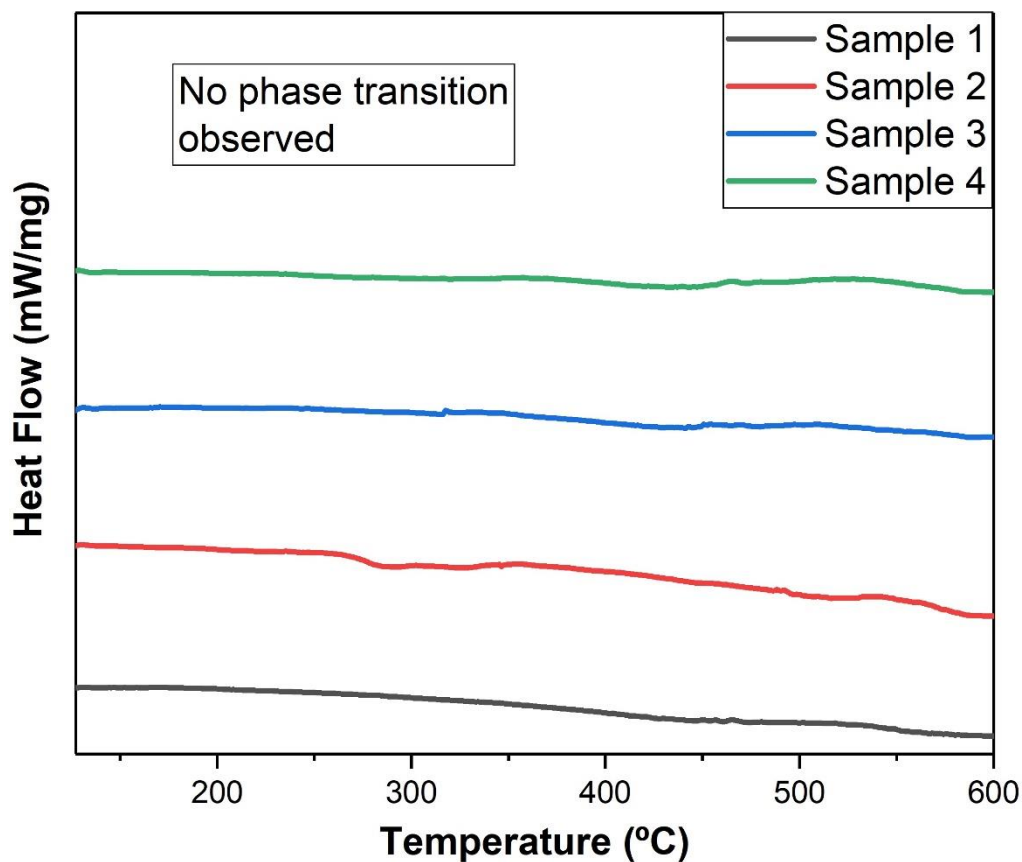


Figure 4.16: DSC Profile

4.7 X-Ray Diffraction (XRD)

XRD analysis was performed to observe any phase change or presence of any impurity. The diffraction profile was taken from 30° - 75°.

The elemental homogeneity of the alloys were determined by XRD. The XRD patterns obtained are shown in Figure 4.17. From the XRD results, we can

see that all the four alloys have almost the same constitution. The presence of both α and β peaks is evident in all the four samples, but the intensity of the α peak became stronger as the Zr content was increased, which implies that the α -phase became more stable as the Zr content was increased in the alloy.

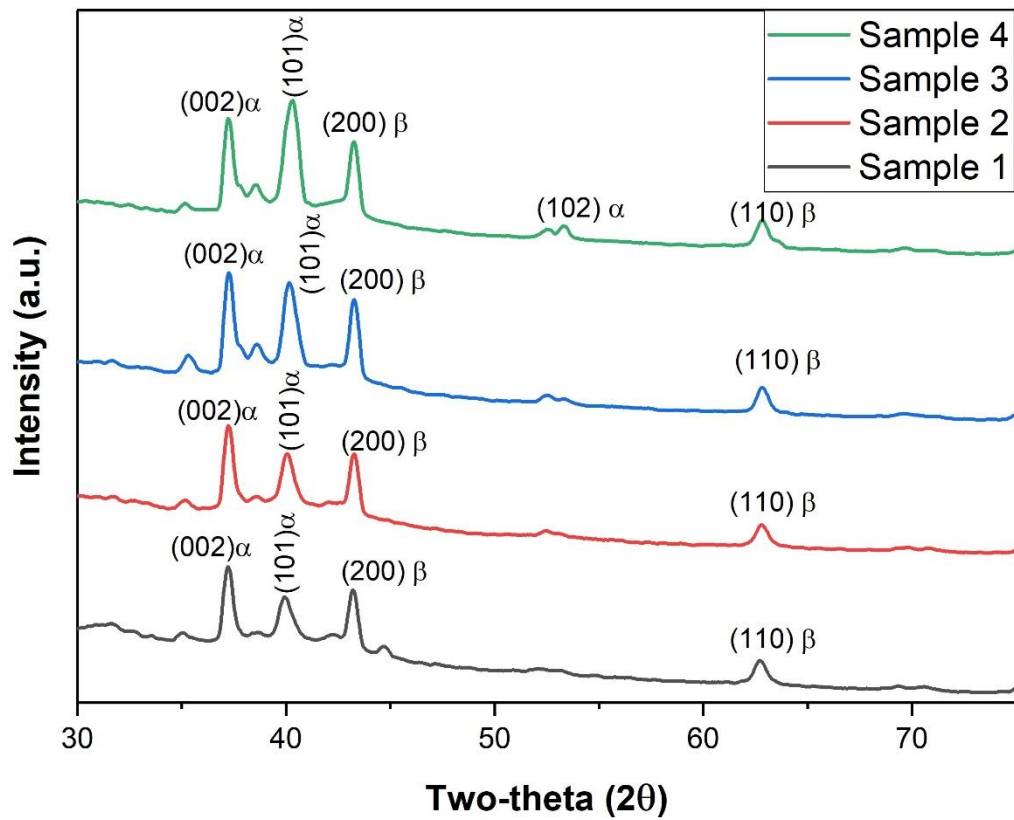


Figure 4.17: XRD Result

A summary of the mechanical properties obtained in this study are shown in Table 4.6. The variation of the mechanical properties depends on the change in amount of Zr content in each sample.

Table 4.6: Summary of results

Sample	Yield strength (MPa)		Tensile strength (MPa)		Elongation at RT (%)	Rockwell Hardness (HRC)
	24 °C	500 °C	24 °C	500 °C		
Sample 1	620 ± 10	490 ± 10	785 ± 10	551 ± 10	12 ± 0.5	26.7 ± 0.2
Sample 2	660 ± 10	-	790 ± 10	-	12.4 ± 0.5	29.5 ± 0.2
Sample 3	685 ± 10	-	823 ± 10	-	13.1 ± 0.5	32.7 ± 0.2
Sample 4	957 ± 10	750 ± 10	1067 ± 10	850 ± 10	13.7 ± 0.5	34.3 ± 0.2

Chapter 5 CONCLUSION

This thesis explored the effect of zirconium addition on the mechanical properties of titanium. Four alloys with zirconium concentration of 2%, 4%, 6% and 8% were prepared for the study. The relationship between microstructure and the mechanical properties of titanium alloy (after zirconium addition) has also been discussed.

Overall, the testing shows that the alloy Ti-6Al-8Zr-2Sn-0.5Mo-0.5Nb-0.3Si can be used safely in aircraft turbine compared to the Ti-6Al-2Zr-2Sn-0.5Mo-0.5Nb-0.3Si alloy, as the former has higher strength than the latter.

- Microscopic evaluation of the alloys revealed lamellar α phase structures, which became finer with increase in Zr content (2-8 %). This has increased the restriction to deformation in the alloy, benefiting its mechanical properties.
- Hardness value of the alloys increased with increase in Zr content.
- The tensile strengths of the alloys also increased with increase in zirconium content.
- As expected, increase in temperature decreased the tensile properties of the alloys. The ultimate tensile strength was reduced by 20% in the higher zirconium content alloy in comparison with 29% reduction in the lower zirconium content alloy.
- The wear loss increased linearly with increase in applied load.
- No phase transitions were observed in any of the alloys up to 600 °C.
- The phases present in the alloy were identified. It was also observed that the α -phase became more stable with increase in Zr content.

Overall, the results show an increased effect on the mechanical properties of titanium after zirconium addition. The Ti-6Al-8Zr-0.5Mo-0.5Nb-0.3Si alloy might be a suitable candidate for high temperature applications.

5.1 Future Scope of this study

Attempt has been made here to study the effect of zirconium addition on the characteristics of titanium alloy at room temperature and at high temperature. Many of the challenges and assumptions in testing have been addressed. This thesis and the data collected may help fill voids in aircraft industry, where conventional titanium alloys are being used. Many works have been initiated here, but restricted due to the unavailability of resources. So, there is still scope for further research and development in this area, like using different types of alloying addition mechanisms, or studying the effect of other elements for alloying addition in place of zirconium.

REFERENCES

1. Pollock, T.M. (2016), Alloy design for aircraft engines, *Nature Materials*, 15, 809.
2. Zhou, Y., et al. (2009), Influence of Zr content on phase transformation, microstructure and mechanical properties of Ti_{75-x}Nb₂₅Zr_x (x=0–6) alloys, *Journal of Alloys and Compounds*, 486, 628-632.
3. UNIVERSITYofNewYork (2016), <http://www.essentialchemicalindustry.org/metals/titanium.html>
4. Higgins, R.A. (2010), *Materials for engineers and technicians*, Routledge.
5. Leyens, C. and M. Peters (2003), *Titanium and titanium alloys fundamentals and applications*, Wiley-VCH, Weinheim.
6. J. Donachie, M. and S. J. Donachie (2002), *Superalloys: A Technical Guide*, 2nd Edition.
7. Welsch, G., R. Boyer, and E. Collings (1993), *Materials properties handbook: titanium alloys*, ASM international.
8. Collings, E. (1984), *The physical metallurgy of titanium alloys*, Metals Park Ohio, 3.
9. Polmear, I., et al. (2017), *Light alloys: metallurgy of the light metals*, Butterworth-Heinemann.
10. Semiatin, S.L., V. Seetharaman, and I. Weiss (1997), The thermomechanical processing of alpha/beta titanium alloys, *JOM*, 49, 33-39.
11. Fushimi, K., K. Azumi, and M. Seo (2000), Use of a Liquid-Phase Ion Gun for Local Breakdown of the Passive Film on Iron, *Journal of The Electrochemical Society*, 147, 552-557.
12. Villars, P., A. Prince, and H. Okamoto *Handbook of Ternary Alloy Phase Diagrams* (ASM International, Materials Park, OH, 1995), Google Scholar.

13. Hu, D., et al. (2006), Sulphide/phosphide precipitation associated with carbon saturation in Ti–15V–3Cr–3Sn–3Al–0.2 C, *Journal of alloys and compounds*, 413, 77-84.
14. Weiss, I. and S.L. Semiatin (1998), Thermomechanical processing of beta titanium alloys—an overview, *Materials Science and Engineering: A*, 243, 46-65.
15. Sieniawski, J., et al. (2013), Microstructure and mechanical properties of high strength two-phase titanium alloys.
16. Oliveira, V., et al. (1998), PREPARATION AND CHARACTERIZATION OF Ti-Al-Nb ALLOYS FOR ORTHOPEDIC IMPLANTS, *Brazilian Journal of Chemical Engineering*, 15, 326-333.
17. Lütjering, G. (1998), Influence of processing on microstructure and mechanical properties of ($\alpha+\beta$) titanium alloys, *Materials Science and Engineering: A*, 243, 32-45.
18. Namboodhiri, T.K.G., C.J. McMahon, and H. Herman (1973), Decomposition of the α -phase in titanium-rich Ti-Al alloys, *Metallurgical Transactions*, 4, 1323-1331.
19. Van Thyne, R.J. and H.D. Kessler (1954), Influence of Oxygen, Nitrogen, and Carbon on the phase relationships of the Ti-Al system, *JOM*, 6, 193-199.
20. Hari Kumar, K.C., P. Wollants, and L. Delacy (1994), Thermodynamic assessment of the Ti-Zr system and calculation of the Nb-Ti-Zr phase diagram, *Journal of Alloys and Compounds*, 206, 121-127.
21. Lütjering, G. and J.C. Williams (2007), *Titanium*, Springer Science & Business Media.
22. Eylon, D., et al. (2013), High-Temperature Titanium Alloys—A Review.
23. Lütjering, G. and J. Williams (2007), *Titanium* 2nd edition (Berlin-New York, Springer).
24. Oldani, C. and A. Dominguez (2012), Titanium as a Biomaterial for Implants, *InTech*.
25. Acero, J., et al. (1999), The behaviour of titanium as a biomaterial: microscopy study of plates and surrounding tissues in facial osteosynthesis, *Journal of cranio-maxillo-facial surgery*, 27, 117-123.

26. Sarmiento, A., et al. (1979), Clinical experiences with a titanium alloy total hip prosthesis: a posterior approach, *Clinical orthopaedics and related research*, 166-173.
27. Rao, S., et al. (1996), Effect of Ti, Al, and V ions on the relative growth rate of fibroblasts (L929) and osteoblasts (MC3T3-E1) cells, *Bio-medical materials and engineering*, 6, 79-86.
28. Albrektsson, T. and C. Johansson (2001), Osteoinduction, osteoconduction and osseointegration, *European Spine Journal*, 10, S96-S101.
29. Adell, R., et al. (1981), A 15-year study of osseointegrated implants in the treatment of the edentulous jaw, *International Journal of Oral Surgery*, 10, 387-416.
30. International, A.S.M. and C. Handbook (1991), <http://products.asminternational.org/hbk/do/navigate?navOn=true&src=/content/V04/D00/A01/index.html>
31. Halley-Demoulin, I., D. Ciosmak, and M. Lallemand (1994), Oxydation des alliages TiZr sous air et sous oxygène II. Rôle de la composition des alliages sur l'évolution cinétique et morphologique du titane au zirconium, *Journal of alloys and compounds*, 204, 133-143.
32. Donachie, M.J. (2000), *Titanium: a technical guide*, ASM international,
33. Hosamani, L., W. Wood, and J. Devletian (1989), SOLIDIFICATION OF ALLOY 718 DURING VACUUM ARC REMELTING WITH, *Superalloy 718: metallurgy and applications: proceedings of the International Symposium on the Metallurgy and Applications of Superalloy 718*, 49.
34. Huy, N. (2009), NT Huy, YK Huang, and A. de Visser, *J. Magn. Magn. Mater.* 321, 2691 (2009), *J. Magn. Magn. Mater.*, 321, 2691.
35. Zhecheva, A., et al. (2005), Enhancing the microstructure and properties of titanium alloys through nitriding and other surface engineering methods, *Surface and Coatings Technology*, 200, 2192-2207.
36. Zhang, D.L. (1996), Precipitation of Excess Silicon during Heat Treatment of Cast Al-7wt%Si-0.4wt%Mg Alloy, *Materials Science Forum*, 217-222, 771-776.

37. Chandler, H. (1999), Hardness testing. 2nd edition, ASM International, Materials Park, OH (US).
38. PACETechnologies (2006-2017), <http://www.metallographic.com/Etchants/Etchants.htm>
39. Kumar, D., et al. (2017), Fretting fatigue stress analysis in heterogeneous material using direct numerical simulations in solid mechanics, Tribology International, 109, 124-132.
40. Yue, T. and M.A. Wahab (2017), Roughness Effects on Fretting Fatigue, Journal of Physics: Conference Series, 012056.
41. Neale, M. and M. Gee (2001), A guide to wear problems and testing for industry, William Andrew.
42. Bhushan, B. and B.K. Gupta (1991), Handbook of tribology: materials, coatings, and surface treatments.
43. Attia, M.H. and R.B. Waterhouse (1992), Standardization of fretting fatigue test methods and equipment, ASTM International.
44. Archard, J. (1953), Contact and rubbing of flat surfaces, Journal of applied physics, 24, 981-988.
45. Archard, J. and W. Hirst (1956), The wear of metals under unlubricated conditions, Proc. R. Soc. Lond. A, 236, 397-410.
46. BBS, <https://www.bbshalmstad.se/en/infocenter/hardness-conversion-table/>
47. CarbideDepot, <http://www.carbidedepot.com/formulas-hardness.htm>
48. OnlineMetals, <https://www.onlinemetals.com/hardness.cfm>